

Full length article

Digital twins probe into food cooling and biochemical quality changes for reducing losses in refrigerated supply chains



Thijs Defraeye^{a,*}, Giorgia Tagliavini^{a,b}, Wentao Wu^{b,c,d}, Kevin Prawiranto^{a,b}, Seraina Schudel^{a,e}, Mekdim Assefa Kerisima^{f,g}, Pieter Verboven^f, Andreas Bühlmann^e

^a Empa, Swiss Federal Laboratories for Materials Science and Technology, Laboratory for Biomimetic Membranes and Textiles, Lerchenfeldstrasse 5, CH-9014, St. Gallen, Switzerland

^b Chair of Building Physics, ETH Zurich, Stefano-Francini-Platz 5, 8093, Zürich, Switzerland

^c Empa, Swiss Federal Laboratories for Materials Science and Technology, Multiscale Studies in Building Physics, Überlandstrasse 129, 8600, Dübendorf, Switzerland

^d Harvard Center for Green Buildings and Cities, Harvard Graduate School of Design, Harvard University, Cambridge, MA, 02138, United States

^e Agroscope, Plants and Plant Product Division, Müller-Thurgau-Strasse 29, 8820, Wädenswil, Switzerland

^f MeBioS – Postharvest Group, Department of Biosystems, KU Leuven, Willem de Croylaan 42, 3001, Heverlee, Belgium

^g Addis Ababa Institute of Technology, Addis Ababa University, King George VI St, Addis Ababa, 1000, Ethiopia

ARTICLE INFO

Keywords:
Thermophysical
Fruit simulator
Multiphysics
In-silico
Biophysical twin
Digital avatar

ABSTRACT

Refrigerated transport and storage of mango fruit are essential to maintain quality, reduce food waste and the associated embodied energy losses. Refrigeration is also key to enable successful transcontinental export to distant markets. To minimize the environmental impact of the cold chain and to optimize logistics, a better knowledge of the fruit quality evolution within individual shipments would be extremely valuable. For this purpose, a digital fruit twin is developed, based on mechanistic modeling. This digital twin simulates the thermal behavior of mango fruit throughout the cold chain, based on the measured environmental temperature conditions, namely the air temperature in the vicinity of the fruit. At the same time, the evolution of associated quality attributes, due to enzymatically-driven, temperature-dependent biochemical degradation reactions, is quantified. Also, a biophysical counterpart of real mango fruit – an innovative fruit simulator sensing device – was developed and used for model validation of fruit pulp temperatures. We identified – in-silico – the impact of the unique delivery air temperature history and cold chain length on fruit quality evolution for actual maritime vs. airfreight transport pathways. Digital twins were found to provide complementary insights in the thermophysical behavior of fruit, particularly in supply chains of very perishable species, and for storage at low airflow rates. Such mechanistic modeling enabled to understand, record, and predict where temperature-dependent fruit quality loss occurs in each supply chain. In that way, digital twins can help to improve refrigeration processes and logistics to reduce food losses, thereby making the refrigerated supply chain greener.

1. Introduction

Fresh mango is a popular fruit for domestic consumption as well as consumption in non-producing countries. This fruit grows predominantly in Asia and South America. The production was around 50 million tons worldwide in 2017 (FAO, 2018), but note that this data inherently also includes mangosteen and guava. However, over the past years, the import of this tropical fruit into non-producing countries has increased exponentially. As an example, 328,000 tons of mangos, mangosteens and guavas were imported into Europe in 2006 while in 2016, over 580,000 tons were imported, with a total value of 1.13

billion USD (FAO, 2018). As such, the transcontinental transportation of mangos often relies on refrigeration via airfreight or maritime transport in containers or ships. The main exporting countries are Mexico, India, Thailand, Peru and Brazil (FAO, 2018). The environmental impact of these fruit imports (National Mango Board, 2010), and the associated embodied energy and greenhouse gas emissions are huge. This makes it imperative to optimize the cold chains to preserve quality, extend shelf life and minimize losses. The postharvest losses in the overall fresh produce supply chain vary between 13% in Europe and 38% in sub-Saharan Africa (Gustavsson et al., 2011).

Cooling this climacteric fruit after harvest and keeping them

* Corresponding author at: Empa, Swiss Federal Laboratories for Materials Science and Technology, Laboratory for Biomimetic Membranes and Textiles, Lerchenfeldstrasse 5, CH-9014 St. Gallen, Switzerland.

E-mail address: thijs.defraeye@empa.ch (T. Defraeye).

refrigerated throughout the rest of the supply chain is essential because the temperature is a key parameter affecting fruit quality attributes (Robertson, 2016; Thompson, 2004). Meanwhile, low-temperature damage, such as chilling injury, should be avoided. This challenging task of maintaining a proper cold chain, with an often, narrow temperature window, requires optimal control of the convective cooling processes, supply chain logistics, and ventilated packaging design. To do so in a targeted way, we need to have quantitative insight into the mango fruit cooling process and the associated evolution of the quality attributes throughout transcontinental supply chains.

Much experimental research has been done on mango cooling and storage, mainly focusing on postharvest treatments, such as controlled atmosphere storage (Brecht et al., 2003a; Nakamura et al., 2004), modified atmosphere packaging and fruit coating (Baldwin et al., 1999; Pesis et al., 2000; Rao and Shivashankara, 2014), 1-methylcyclopropane application as a competitive ethylene inhibitor (Ngamchuachit et al., 2014; Sivakumar et al., 2012)), or the cooling process itself (De Mello Vasconcelos et al., 2019). The impact of these treatments on several quality attributes have been measured, including pulp and peel firmness, soluble solids content (SSC), titratable acidity (TA), flesh and peel color, and antioxidants (e.g., phenolic and flavonoid content) or vitamin content. Also, the incidence of physiological damage, such as chilling injury, has been investigated (Cantre et al., 2017; Dea et al., 2010; Mohammed and Brecht, 2002). However, less attention was given to the key boundary condition for quality attribute decay, namely temperature (Emongor, 2015; Nunes et al., 2007). Only the air temperature was measured here, even though the fruit pulp temperature also plays a key role since it lags due to thermal inertia.

As an alternative to experiments, mechanistic modeling by finite element or finite volume simulations could provide complementary insight into different biophysical processes (Casado et al., 2017; Copelli et al., 2019; Nordio et al., 2019; Radu et al., 2014; Sitaraman et al., 2015), including the convective cooling inside the fruit and the thermal exchange with its environment. Outputs of such simulations include thermal data at every location in space and time. Several valuable computational studies have been performed on various fruit, including apple, banana or grapes (Ambaw et al., 2013; Dehghannya et al., 2010; Norton et al., 2013), but still, present specific limitations. Firstly, the temperature history has been linked to overall fruit storage life (Wu et al., 2018; Wu and Defraeye, 2018), but not to single quality attributes, such as firmness or vitamin content, which are driven by temperature-dependent biochemical reactions. Secondly, the impact of the complex shape of mango fruit and its internal features (seed) on the thermal and biochemical processes has not yet been identified (Gruyters et al., 2018). Typically, mangos are represented as ellipsoids (without seed), for example, when analyzing hot water treatment (Marcelo et al., 2018; Mendoza Orbegoso et al., 2017). Thirdly, idealized cold chain scenarios have been targeted, which do not reflect the fluctuations in temperature and duration of actual individual transcontinental cold chains and their impact on storage life variability.

This study aims at mitigating these hurdles by creating a validated digital twin of fruit with a complex shape and composition, namely a

mango. A digital twin is defined as a virtual representation of the real-world counterpart of an object, which (1) contains all its elements, (2) simulates accurately and realistically all relevant processes and process kinetics, and (3) is connected/linked to the real-world processes by sensor data input, preferably in real-time. By 2021, 50% of the large industrial companies are estimated to rely on digital twins, leading to an expected 10% gain in effectiveness (Gartner, 2019a, 2019b). Applied to mango fruit, its digital twin contains all components (seed, pulp) and simulates the physical cooling behavior and the associated evolution of biochemical-driven fruit quality attributes throughout the postharvest supply chain. By using measured air temperature data in the vicinity of the fruit as an input, actual transcontinental supply chains can be mimicked in-silico. In this study, the underlying model for the digital twin is a mechanistic, first-principles-based one, using finite elements. Other options are to use statistical models or data-driven models based on machine learning (Gwanpua et al., 2015). We opted for mechanistic modeling, since such physics-based models provide temperatures at each point in time and space (in the fruit), thereby enabling to quantify volume-averaged fruit temperatures or surface heat fluxes.

With this mechanistic finite element model, we identify how cooling at a higher airspeed can improve storage life. We also determine the impact of the unique measured cold chain length and delivery air temperature (DAT) history on the mango fruit quality which the retailer receives, by applying this to two cold chains with different environmental impacts, namely maritime and airfreight transport. We show how the cooling of a real mango fruit differs from that of its equivalent spherical representation, and so how important an accurate shape representation is on the cooling process. These pioneering steps enable us to identify where the quality loss occurs in each single shipment, which is essential to help improve cooling processes and reduce food losses to improve the sustainability of mango supply chains.

2. Materials and methods

2.1. Geometrical model of mango fruit

A three-dimensional geometrical model of mango fruit was generated and used as input for the computational model (section 2.2). It was designed to represent a typical mango of the cultivar Kent, as detailed in the Supplementary Material. Table 1 provides the geometrical specifications of the mango fruit and seed. The volume of the fruit pulp equals the total volume of the fruit, as stipulated in Table 1, minus that of the seed. An equivalent sphere was defined for the mango fruit and the seed, separately, by matching their volumes. Similarly, equivalent ellipsoids were also defined (detailed in section 2.2). All these equivalent geometrical representations match the volume of the mango fruit and seed (grey cells in Table 1) within 0.01%. The equivalent sphere has a diameter of 99 mm. This diameter was taken as the corresponding length scale (L_{ref} [m]) for the mango fruit in this study since it can be directly calculated from the fruit volume. The peel was not included in the model, as its impact on the cooling kinetics is limited. The reason is

Table 1
Geometrical characteristics of mango fruit and other geometrical representations.

		L (x) mm	W (y) mm	H (z) mm	Volume mm ³ (L/10 ⁶)	Surface area mm ²
Mango fruit	Fruit	119.00	99.00	84.00	504574	31289
	Seed (ellipsoid)	50.40	34.00	24.00	21534	4030
Equivalent sphere	Fruit	98.77	98.77	98.77	504515	30648
	Seed	34.52	34.52	34.52	21531	3743
Ellipsoid (3D)	Fruit	115.87	99.00	84.00	504527	31098
	Seed (ellipsoid)	50.40	34.00	24.00	21534	4030
Ellipsoid (axisymmetric)	Fruit	115.87	91.19	91.19	504503	30948
	Seed (ellipsoid)	50.40	28.57	28.57	21533	3938

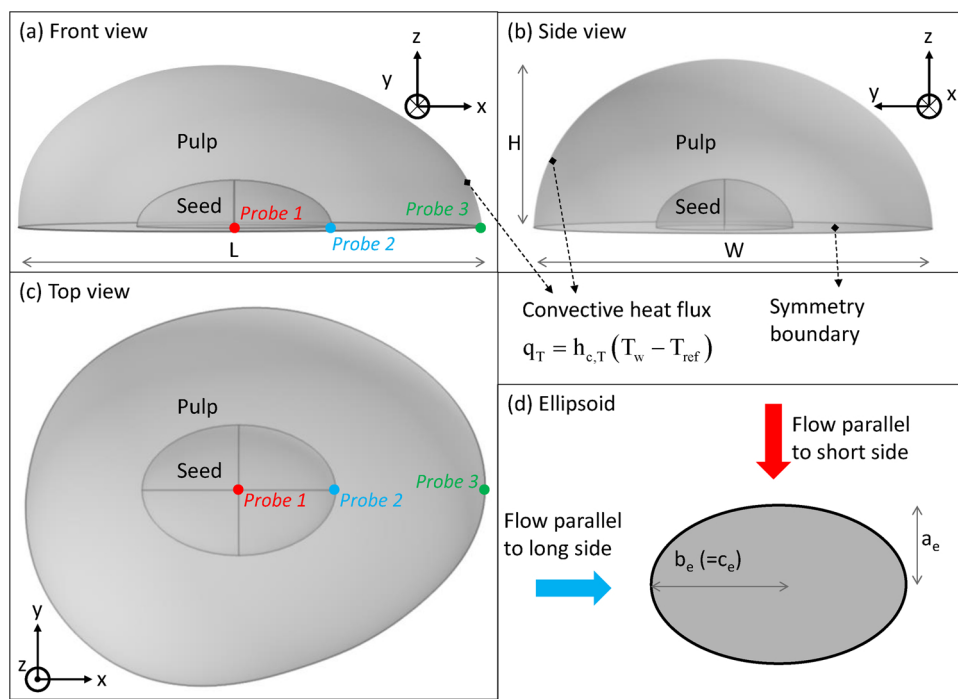


Fig. 1. Computational model of mango fruit (half fruit shown due to symmetry) with boundary conditions (a–c). Ellipsoid with indication of dimensions (d).

Table 2

Thermal properties of mango components of pulp and seed.

		Mass fraction [%]	Density [kg m ⁻³]	Specific heat capacity [J kg ⁻¹ K ⁻¹]	Thermal conductivity [W m ⁻¹ K ⁻¹]	Thermal diffusivity (x 10 ⁶) [m ² s ⁻¹]	Source
Pulp	Total	–	932	3665	0.445	0.130	Calculated based on composition from ASHRAE (2010)
Pulp	Components						
	Water	81.71	996	4129	0.604	0.1468	ASHRAE (2010)
	Protein	0.51	1320	2032	0.202	0.0752	ASHRAE (2010)
	Fat	0.27	917	2012	0.175	0.0949	ASHRAE (2010)
	Carbohydrates	17.00	1593	1586	0.227	0.0900	ASHRAE (2010)
	Ash	0.50	2418	1129	0.356	0.1306	ASHRAE (2010)
	Air	0 (but porosity = 12.7%)	1.225	1006	0.0242	19.6	Defraeye (2011)
Seed	Total	–	1105	2805	0.367	0.118	Calculated based on composition from ASHRAE (2010)
Seed	Components						
	Water	45.2	996	4129	0.604	0.1468	Nzikou et al. (2010)
	Protein	6.36	1320	2032	0.202	0.0752	Nzikou et al. (2010)
	Fat	13	917	2012	0.175	0.0949	Nzikou et al. (2010)
	Carbohydrates	32.24	1593	1586	0.227	0.0900	Nzikou et al. (2010)
	Ash	3.2	2418	1129	0.356	0.1306	Nzikou et al. (2010)
	Air	0 (but porosity = 5%)	1.225	1006	0.0242	19.6	Defraeye (2011)

that it is rather thin and its thermal properties are in the same order of magnitude as those of the fruit pulp.

2.2. Continuum multiphysics model

A continuum multiphysics model was developed to calculate heat transport inside this composite fruit and its convective exchange with the environment throughout the cold chain (Fig. 1). The associated evolution of multiple temperature-dependent quality attributes, which are the result of biochemical reactions in the fruit pulp, was also predicted. The geometrical configuration used to evaluate the thermal history of mango fruit throughout the cold chain was chosen to be a single mango fruit, exposed to convective cooling. This configuration simplified the actual conditions to some extent, as one single fruit is investigated. Thereby the thermal interaction with other fruit is ignored, which is anyways limited due to the few

contact points, and the fact that surrounding fruit is at a similar temperature. The initial temperature, initial ripeness degree, fruit shape and size, and thermal properties were assumed the same for all cases, but note that all these can differ according to the harvest time and place, and due to the biological variability between individual fruit in a batch. However, the rationale of the present study was to target specific questions about the cooling and quality evolution, and our simplified configuration is sufficient to serve this purpose. The base case, as well as the other variants that are simulated, are detailed below in Section 2.3.

2.2.1. Conservation equation for energy

The energy conservation equation was solved for the dependent variable temperature T [K], to calculate heat conduction in the fruit pulp and seed:

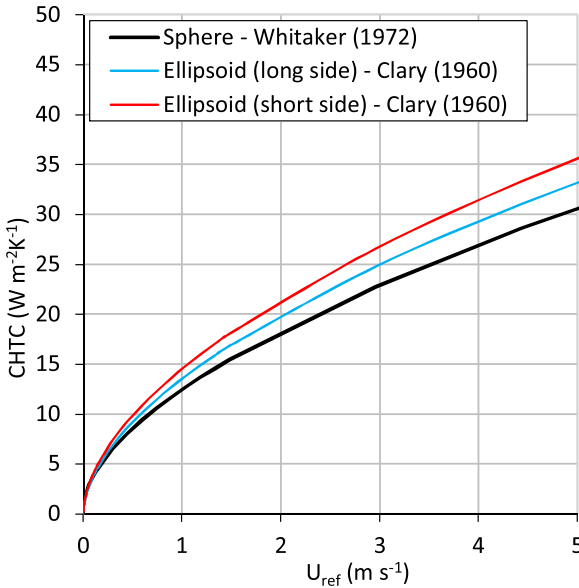


Fig. 2. CHTC correlations as a function of reference air speed for a sphere (Whitaker, 1972), and an axisymmetric ellipsoid with airflow parallel to the long side and the short side (Clary, 1960).

$$\rho_j c_{p,j} \frac{\partial T}{\partial t} + \nabla \cdot (-\lambda_j \nabla T) = Q_{s,j} \quad (1)$$

where subscript j indicates fruit pulp (p) or seed (s), ρ_j is the corresponding density of the fruit pulp or seed [kg m^{-3}], $c_{p,j}$ is the specific heat capacity [$\text{J kg}^{-1} \text{K}^{-1}$], λ_j is the thermal conductivity [$\text{W m}^{-1} \text{K}^{-1}$], t is the time [s] and $Q_{s,j}$ is a volumetric heat source term [W m^{-3}]. This source term represents the heat of respiration [W kg^{-1}], multiplied by the density of the respiring material [kg m^{-3}]. Thermal equilibrium between all components and phases was assumed in the present continuum model.

The material properties are given in Table 2. The data were calculated based on the composition of the different components (ASHRAE, 2010). Based on the volume (Table 1) and density of fruit pulp and seed, the weight of the mango was determined to be 474 g, which is representative for actual Kent mangoes, as verified by our gravimetric measurements on fresh mango fruit (results not reported). The thermal diffusivity is defined as $\alpha_j = \lambda_j / (\rho_j c_{p,j})$ [$\text{m}^2 \text{s}^{-1}$]. These properties were assumed constant, which was sufficient for the scope of this study. The properties, however, can vary slightly with temperature, ripeness degree, harvest location, and harvest year. As such, small differences in thermal properties between different literature sources are present (Bon et al., 2010).

Nonetheless, the sensitivity of the cooling to these small variations is relatively limited (Tagliavini et al., 2019). Mangos are strongly respiring fruit, generating about 40 mW (at 10 °C) up to 170 mW (at 20 °C) for our particular mango fruit ($\approx 0.5 \text{ kg}$, (ASHRAE, 2010; Kader, 1997)). The heat produced by respiration is assumed only to occur in the fruit pulp, so the source term is only applied here. The exact implementation of the heat of respiration is given in the Supplementary Material.

2.2.2. Thermal boundary conditions

The airflow around the fruit was not modeled explicitly, but instead, its impact on the cooling process was accounted for by using a convective heat transfer coefficient (CHTC) [$\text{W m}^{-2} \text{K}^{-1}$], represented as $h_{c,T}$ (Eq. (2)). The boundary condition at the air–fruit interface (continuity of fluxes) was specified as:

$$\mathbf{n} \cdot (-\lambda_p \nabla T) = q_T = h_{c,T} (T_w - T_{ref}) \quad (2)$$

where \mathbf{n} is the unit vector normal to the interface, q_T [$\text{J m}^{-2} \text{s}^{-1}$] is the

heat flux at the interface, and T_w and T_{ref} are the temperatures [K] at the interface and of the approach flow air (DAT), respectively. This boundary condition states that heat loss/gain from the fruit, due to conduction, equals the convective (sensible) heat exchange with the environment. In actual cold chains, the temperature difference between adjacent fruit in the ventilated packaging is usually rather small during cooling. Therefore, radiation exchange between different fruit inside the stack was considered limited compared with convective heat transfer, and hence, radiation was not modeled.

A single CHTC was assumed over the entire fruit surface, as a simplified representation since a spatial CHTC variation can be present over the fruit surface (Defraeye et al., 2013; Tagliavini et al., 2019). Within the scope of the present study, a spatially-constant CHTC was sufficient. The dependency of the CHTC on the speed was accounted for by the following correlation for flow around a sphere (Eq. (3)) or an ellipsoid (Eq. (4)) (Clary, 1960; Whitaker, 1972):

$$Nu = 2 + (0.4Re^{0.5} + 0.06Re^{0.667})Pr^{0.4} \left(\frac{\mu_a}{\mu_{a,\text{wall}}} \right)^{0.25} \quad (3)$$

$$Nu = 0.489Pr^{0.33}Re^{0.557} \left(\frac{a_e}{c_e} \right)^{-0.07} \left(\frac{b_e}{c_e} \right)^{-0.44} \quad (4)$$

where μ_a and $\mu_{a,\text{wall}}$ are the absolute viscosities of the air (subscript a) and the air at the wall, respectively, which were considered as equal in this study ($\mu_a = 1.7894 \times 10^{-5} \text{ kg m}^{-1} \text{s}^{-1}$) as the air properties were assumed constant; Pr is the Prandtl number ($Pr = \nu_a/\alpha_a$), which was 0.744 in the present study. Here, ν_a is the kinematic viscosity of air [$\text{m}^2 \text{s}^{-1}$], which equals μ_a/ρ_a , Nu is the Nusselt number and equals CHTC $\cdot L_{ref}/\lambda_a$, where λ_a is the thermal conductivity of air ($0.0242 \text{ W m}^{-1} \text{K}^{-1}$). The Reynolds number (Re) was based on the airspeed of the approach flow (U_{ref}) and length scale of the mango fruit (L_{ref}), so $U_{ref} \cdot L_{ref}/\nu_a$. In Eq. (4), a_e is the length of the major principal semi-axis of the ellipsoid perpendicular to the fluid flow [m] (Fig. 1), b_e is the length of the horizontal principal semi-axis of the ellipsoid perpendicular to the major axis and parallel to the fluid flow [m], and c_e is the length of the vertical axis of the ellipsoid perpendicular to the major axis and fluid flow [m], which equals b_e for an axisymmetric ellipsoid (Clary, 1960). Note that these empirical correlations were derived for forced convection, so buoyancy effects were not explicitly accounted for, as these are dependent on the temperature difference between the air and the fruit. The sphere correlation was derived for a very broad Re range, but the ellipsoid correlation was derived for high Re (about 1×10^3 – 1×10^5) and Nu numbers (about 100–400). Fig. 2 shows the correlations for a sphere and an axisymmetric ellipsoid with flow parallel to the long side of the fruit ($b_e = L/2$ of an axisymmetric ellipsoid = 57.94 mm, Table 1, Fig. 1) and parallel to the short side ($a_e = L/2$ of the axisymmetric ellipsoid = 45.59 mm).

When comparing the correlations, the CHTC values for the ellipsoid for flow parallel to the short axis are within 15% of those of the sphere. An even better agreement is found for flow parallel to the long side of the ellipsoid. Unless specified otherwise, the spherical correlation was applied since (1) it is more generally known, (2) more correlations are available in literature, (3) these correlations have been derived over a large Re range and (4) the length scale is also more easily defined via a single parameter, namely the (equivalent) sphere diameter ($L_{ref} = 99 \text{ mm}$, Table 1). This approach also facilitated deriving a representative CHTC when evaluating different geometrical simplifications (Section 2.3).

2.2.3. Modeling fruit quality attributes

To predict the evolution of multiple quality attributes of the mango fruit, which are temperature dependent, throughout the cold chain, kinetic rate law models were implemented. These attributes include firmness (Firm [N]), soluble solids content (SSC [$^\circ\text{Brix}$]), titratable acidity (TA [% citric acid]), vitamin C (vitC [mg/100 ml]) and beta-

Table 3

Kinetic-rate-law model parameters of quality attributes of mango fruit.

Parameter	Symbol	Unit	SL-TR	SL-MG	Firm	SSC	vitC	TA	BC
Initial value	A ₀		A _{sl,tr} 1	A _{sl,mg} 1	A _f 41.09 N	A _{ssc} 4.10 °Brix	A _{vitC} 114% citric acid	A _{ta} 0.768 mg/100ml	A _{bc} 0.302 mg/100ml
Integration constant	C	–	0	0	0	0	0	0	0
Order of reaction	n	–	1	1	1	1	1	0	0
Activation energy	E _a	J/mol	74268	74268	80830	52284	54074	54184	64385
Constant	k ₀	1/s	306723097	76680774	120309426	−1668	2335	2216	−1747866
Q ₁₀ value	Q ₁₀	–	3.00	3.00	2.99	2.03	2.08	2.08	2.39

Firm: firmness, SSC: soluble solids content, TA: titratable acidity, vitC: vitamin C, BC: beta carotene, SL-TR: storage life of ripe mangos, SL-MG: storage life of mature green mangos.

carotene (BC [mg/100 ml]). The kinetic rate law models quantify the change of each of these specific quality attributes A_i (Robertson, 2016; Van Boekel, 2008):

$$\frac{-dA_i}{dt} = k_i A_i^{n_i} \quad (5)$$

where the subscript i indicates the specific attribute (e.g., firmness), k_i is the corresponding rate constant [s^{−1}], and n_i is the order of the reaction. The order of the reaction is dependent on the attribute's decay kinetics. Examples of zero-order reactions are browning as a result of the Maillard reaction, lipid oxidation, and enzymatic degradation (Robertson, 2016; Van Boekel, 2008). A typical first-order reaction is vitamin loss. Many quality attributes, such as firmness or SSC, actually depend on a multitude of biochemical reactions occurring in the fruit during ripening, of which the effect is lumped into a single attribute, serving as a measure for the ripeness degree. Also, these attributes can be successfully described with rate law models.

This ordinary differential equation (Eq.(5)) is solved. For a constant value of k, that is, at a constant temperature (as detailed below), the quality attribute decreases linearly over time (for zero-order reactions), where the magnitude of the slope equals k, or shows an exponential decrease (for first-order reactions):

$$A_i(t) = A_{0,i} - k_i(T)t \quad (6)$$

$$A_i(t) = A_{0,i} e^{-k_i(T)t} + C_i \quad (7)$$

where A_{0,i} is the quality attribute at the start of the cooling process (t = 0 s) for a specific attribute i and C_i is an integration constant.

However, the rate constant k_i is not constant, and so Eq. (5) needs to be explicitly solved over time. The temperature dependency of the quality attribute was incorporated into the rate constant through an Arrhenius relationship (Robertson, 2016):

$$k_i(T) = k_{0,i} e^{\frac{-E_{a,i}}{RT}} \quad (8)$$

where k_{0,i} is a constant [s^{−1}], E_{a,i} is the activation energy [J mol^{−1}], R is the ideal gas constant (8.314 J mol^{−1} K^{−1}), and T is the absolute temperature [K]. The constants k_{0,i} and E_{a,i} were calibrated from quality attribute data as a function of time at (at least) two different temperatures. The exact procedure on how the parameters k₀ and E_a were determined is explained in the Supplementary Material, and the resulting values are given in Table 3.

These data for such calibration were taken from the literature for physiologically mature mangos (Karathi Esther, 2016), but were for another cultivar ('Apple' mango cultivar) because similar data for 'Kent' mango was not available. Physiological maturity implies that the fruit has a green peel, but yellow flesh. These fruit are quite firm, with high acidity and low SSC, and consequently, are of low edible quality. (Gill et al., 2017). For such mangos, the term mature green (MG) is often used, as the mangos are mature, but not yet ripe. Due to the temperature dependency of k_i, the mechanistic model explicitly solved for Eq. (5) and not Eqs. (6) and (7), which are only valid at a constant

temperature. Note that the reported Q₁₀ value is the ratio of the rate constants at temperatures T and T+10 K (=k_{T+10}/k_T) and is typically about 2 to 3, for degradation reactions in fruit (Robertson, 2016; Thompson, 2004).

In addition to these individual quality attributes, a first-order model of the overall fruit quality evolution for MG mangos and tree-ripe (TR) mangos was established, as detailed in the Supplementary Material. This strategy enables estimating the time taken before the actual fruit is considered lost. The corresponding model parameters are also specified in Table 3. As a comparison of the kinetic rate law quality model to address storage life, a comparison with the data from (Nunes et al., 2007) was made (Fig. 3). Here, the storage life of cv. Tommy Atkins and cv. Palmer, which were in a medium-ripe state, was evaluated at different temperatures. The storage life is defined here as the time fruit can be stored at a certain temperature before the quality exceeds a critical threshold. From the data, our model for TR mangos predicts similar trends and a storage life in the same order of magnitude as the experimental data.

The calibrated models enable predicting the temperature-dependent evolution of these quality attributes and storage life for different cold chains, by relying on a representative fruit core-pulp temperature or average fruit temperature (as detailed below), and for a different initial fruit quality after harvest (e.g., firmness). Note that a variation in the storage life is reported in the literature at a certain temperature (Brecht et al., 2003b; Kader, 1997; Nunes et al., 2007; Slaughter, 2009), due to its dependency on the cultivar, harvest location and exact classification

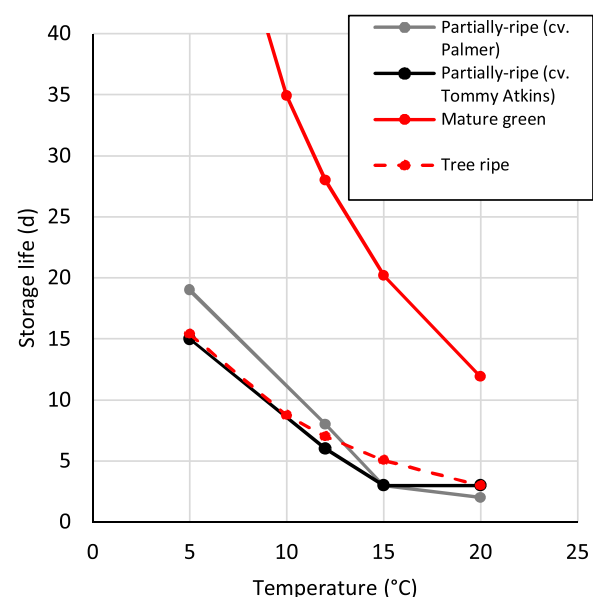


Fig. 3. Storage life as a function of temperature for a kinetic-rate-law model (TR and MG mangos, red lines) and for experiments of (Nunes et al., 2007) on cv. Tommy Atkins and cv. Palmer (black and grey lines).

Table 4

Cooling process conditions for different variants (dash indicates the same conditions as the base case are used).

Name	Ripeness degree	Transport mode	Set temperature	Speed	Time/duration
Base case	MG (+ TR)	Ship	10 °C (CC) + 20 °C (SL)	0.1 m/s	21 d (CC) + 3 d (SL)
1. Operational parameters					
Impact of speed	MG (+ TR)	Ship	–	0.01, 0.1, 1, 10 m/s	–
2. Geometrical simplifications					
3D ellipsoid	MG	Ship	–	–	–
Axisymmetric (2D) ellipsoid	MG	Ship	–	–	–
Sphere	MG	Ship	–	–	–
3. Real CC scenarios					
Ship transport (SA-EU)	MG	Ship	from exp. (7 cases)	–	from exp. (7 cases)
Ship transport (SA-EU)	MG	Ship (low speed)	from exp. (7 cases)	0.01	from exp. (7 cases)
Air transport (SA-EU)	TR	Airfreight	from exp. (12 cases)	–	from exp. (12 cases)

Abbreviations: CC: cold chain, SL: Storage life conditions at retailer, UR: Unripe, SR: Soft ripe; MG: Mature green, TR: Tree ripe, EU: Europe, SA: South America.

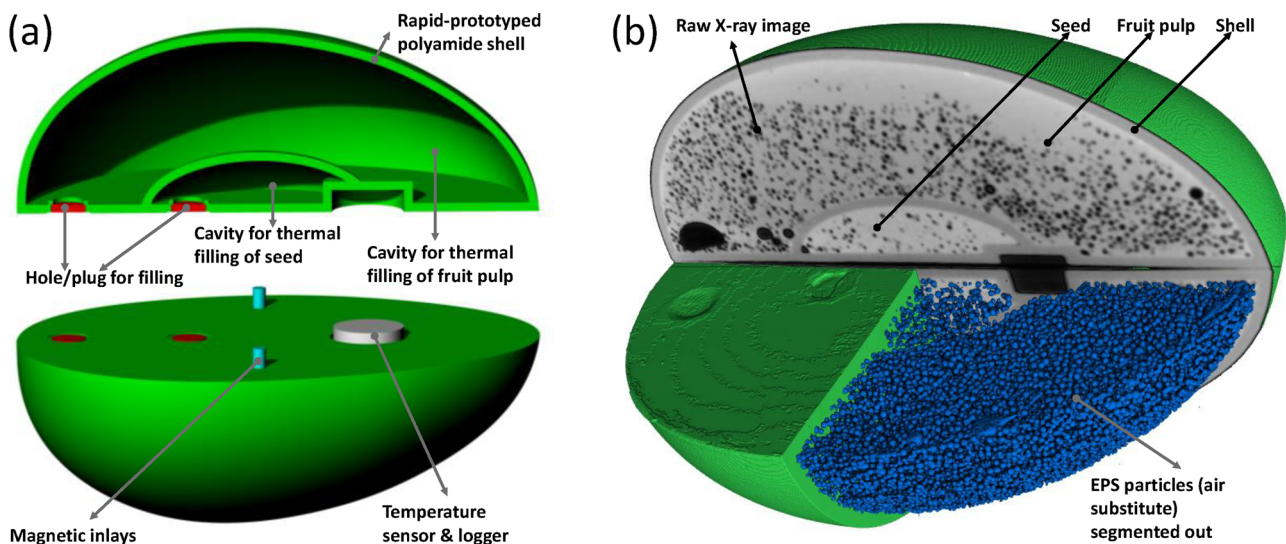


Fig. 4. Physical twin of a mango fruit: (a) CAD model with indication of the various components, (b) cross-section, imaged with X-ray computed tomography, where the EPS particles are segmented out in blue and the shell in green.

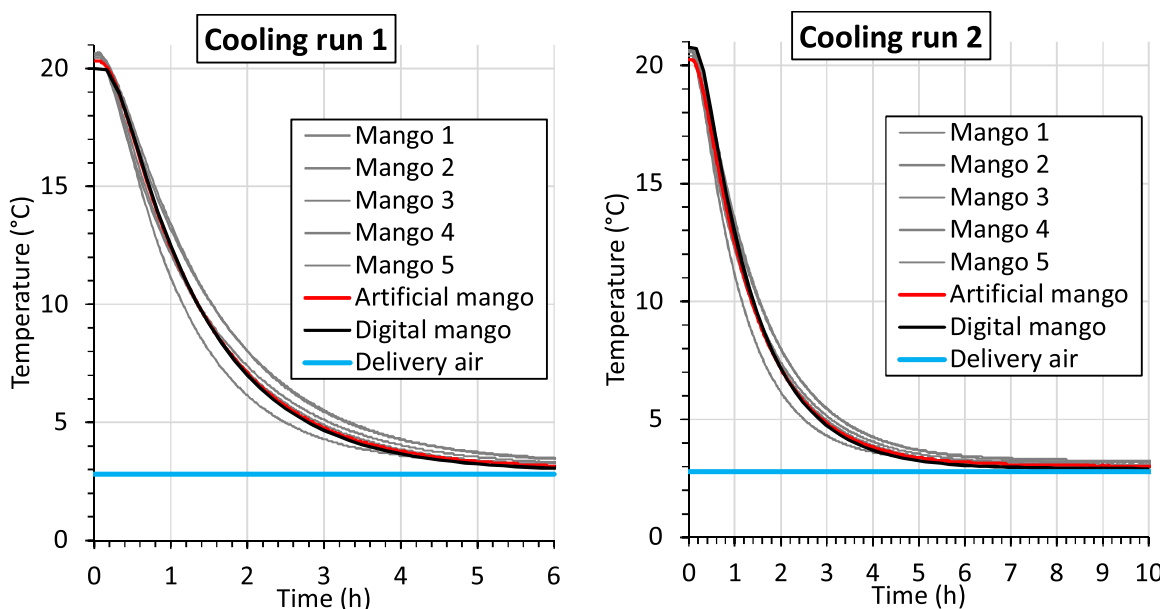


Fig. 5. Core temperature of the mango fruit model (numerical simulations, the artificial fruit simulator and 5 real mango fruit) as a function of time for two cooling runs (similar repetitions). The delivery air temperature (DAT) of the climatic chamber (blue line) is also shown.

of the ripeness. For this study, which is to identify relative differences between treatments for mango fruit, the exact value of the storage life and other quality attribute parameters will not compromise the conclusions regarding the relative differences between cold chains.

2.3. Computational model and configurations

2.3.1. Base case

The base case simulates the cooling down of a mango fruit under constant environmental conditions. The computational model is defined in Fig. 1. Only one of the longitudinal halves of a single mango fruit needed to be modeled, due to symmetry. The relevant material properties are provided in Table 1. The boundary conditions used for modeling are detailed in Fig. 1 and Table 4. The fruit was assumed to be initially (harvested state) at a uniform temperature T_{ini} of 20 °C. The recommended storage conditions for mango fruit are 10 (partially-ripe and ripe) to 13 °C (MG) and relative humidity of 90–95% (Kader, 1997). Therefore, the DAT of the approach airflow was kept at a constant value (T_{ref}) of 10 °C for 21 days of cold storage during a typical overseas cold chain by ship (see section 3.4). We ensured that these conditions were representative of overseas mango transport from South America to

Europe. These conditions were determined from air temperature measurements in several commercial shipments from South America to Switzerland (see Supplementary Material 6). Afterward, the fruit is held at ambient conditions, with a DAT of 20 °C for 3 days, to mimic shelf life conditions at the retailer. In total, 24 days were simulated with this digital twin.

This storage temperature corresponded to that measured in actual mango cold chains (see below), and gives a 10 °C difference between the air and initial fruit temperature. As such, the ratio of the rate constants at these two temperatures equals the Q_{10} value (Table 3). The airspeed for the base case was 0.1 m s⁻¹. This airspeed is representative for vertical airflow within pallets of ventilated boxes of fruit in a refrigerated container (T. Defraeye et al., 2015a, 2015b, 2015c, 2015d; Thijs Defraeye et al., 2015c), but accounting for the fact that local higher airspeeds are found within the stack of porous products due to flow acceleration. This airspeed leads to an average CHTC of 3.8 W m⁻² K⁻¹ (or 4.0 m⁻² K⁻¹ for ellipsoid—long side) on the mango fruit surface (Eqs. (3) and (4)). The corresponding Re , based on the approach airflow speed (U_{ref}) and length scale (L_{ref}) equals 676. Higher airspeeds than that of the base case are also evaluated.

An appropriate grid was constructed for the (half) mango fruit,

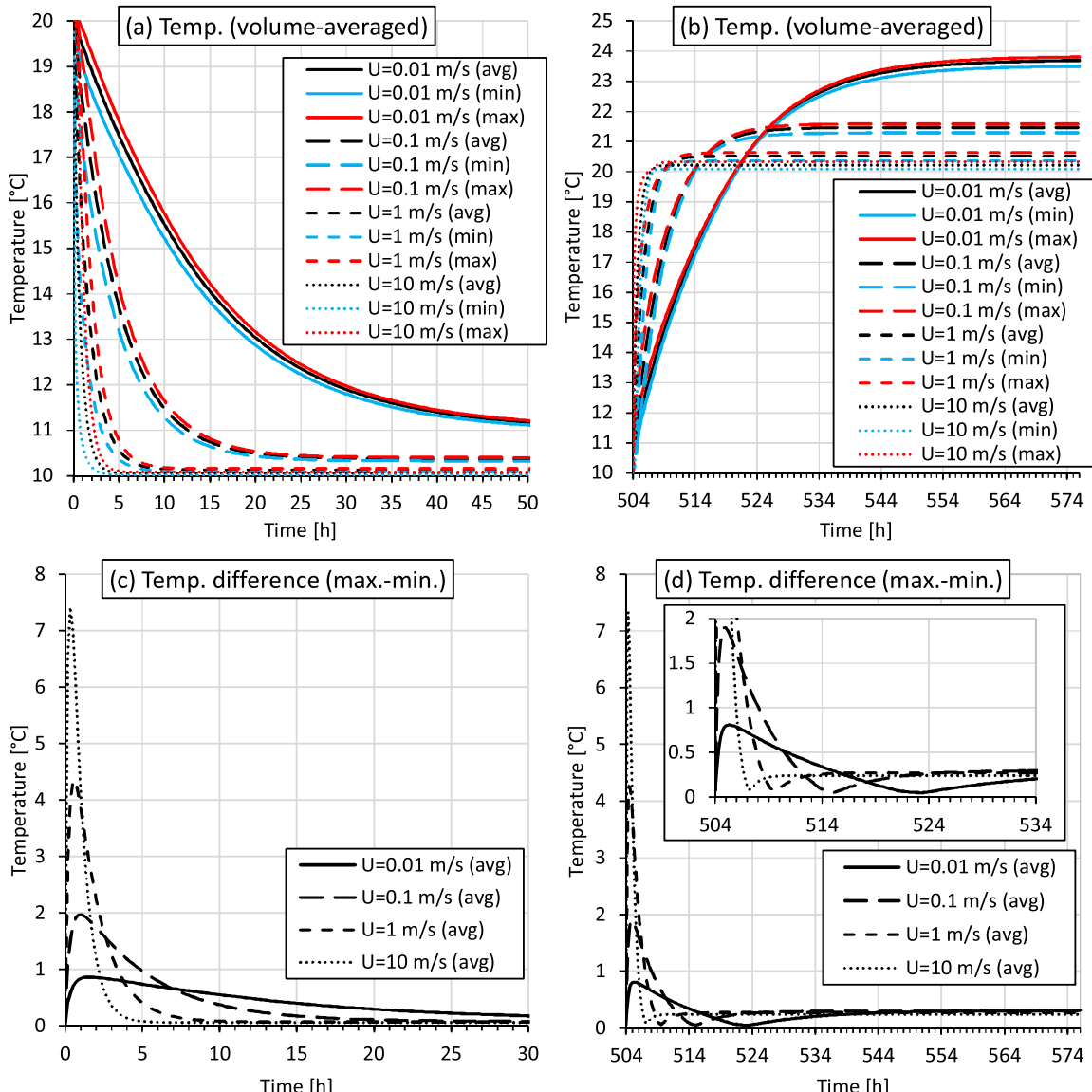


Fig. 6. Volume-averaged fruit temperatures as a function of time during cooling (day 0, (a)) and warming-up period (day 21, (b)) (avg: average, max: maximal, min: minimal, U: speed). Corresponding differences between minimal and maximal volume-averaged temperatures in the fruit (c-d).

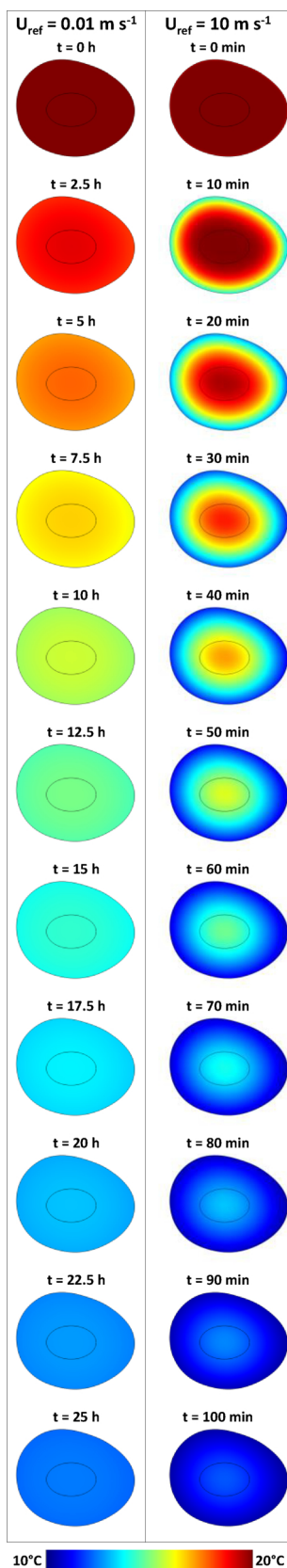


Fig. 7. Color contours of temperature in the central cross section of the mango fruit as a function of time at low and high airflow rates. Different time scales are shown for each flow rate to improve clarity.

based on a grid sensitivity analysis, of which the details can be found in Supplementary Material 8. The spatial discretization error on the local fruit surface and pulp temperatures were estimated to be below 0.01 °C. The grid consists of 9'441 tetrahedral and prismatic finite elements. A gradual refinement toward the air–fruit, and pulp–seed interfaces was applied to enhance numerical accuracy and stability, as the largest gradients occur there, particularly at the start of the cooling process.

2.3.2. Variants

In addition to the base case, various cold chain cases were simulated (Table 4), by varying the process conditions and mango fruit parameters, compared with those of the base case.

- 1 The first type evaluates the impact of various airflow rates.
- 2 The second type evaluates the impact of simplifications of the mango fruit geometry on the cooling kinetics. For all these simplified geometries, the dimensions (Table 1) were determined in such a way that the volume of the fruit and seed were matched to that of the 3D model of the average Kent mango (Fig. 1). These simplifications include an equivalent 3D ellipsoid, an equivalent axisymmetric (two-dimensional) ellipsoid and an equivalent spherical fruit.
- 3 The third type evaluates several realistic mango cold chain scenarios, based on actual air temperature measurements inside the stack of palletized fruits for overseas cold chains via ship and air transport, respectively. These measurements were performed to obtain representative cold chain conditions and to capture the delivery air temperature (DAT) variability between shipments found in practice. Details on these measurements can be found in the Supplementary Material.

2.4. Numerical simulation

This model was implemented in COMSOL Multiphysics (version 5.3a), which is a finite element-based commercial software. Transient conductive heat transfer (Eq. (1)) in the fruit during convective air cooling was solved using the ‘Heat Transfer in Solids’ interface. The kinetic rate law models for the quality attributes (Eq. (5)) were implemented using the ‘Ordinary Differential Equation’ interface. The equations were solved for the dependent variables T , storage life (for ripe and MG mango), firmness, SSC, TA, vitamin C, and beta-carotene. Since the quality attributes do not affect temperature, they could be solved separately after the thermal calculations. Quadratic Lagrange elements were used together with a fully-coupled direct solver, relying on the MUMPS (MULTifrontal Massively Parallel sparse direct Solver) solver scheme. The tolerances for convergence and other solver settings were determined based on sensitivity analysis, in such a way that further increases in the tolerance did not further alter the solution results. These simulations applied adaptive time-stepping, with a maximal time step of 600 s. This time step was determined from sensitivity analysis and ensured a sufficient temporal resolution for the output data. Also, note that such a 10-m time interval is frequently used in the cold chain industry to monitor temperatures during precooling or refrigerated transport. For the real cold chains, a lower maximal time interval between each time step was set within the solver for the simulations (120 s). This time step provided numerical stability, as the sensor input data, which was available every 600 s, often fluctuated strongly.

2.5. Evaluation of cooling rate

The output of the simulations was the mango fruit temperature history for each of the cases and the evolution of fruit quality attributes throughout the cold chain. For the cooling kinetics, the cooling rate of each fruit was assessed from the fruit temperature profiles. For this, the

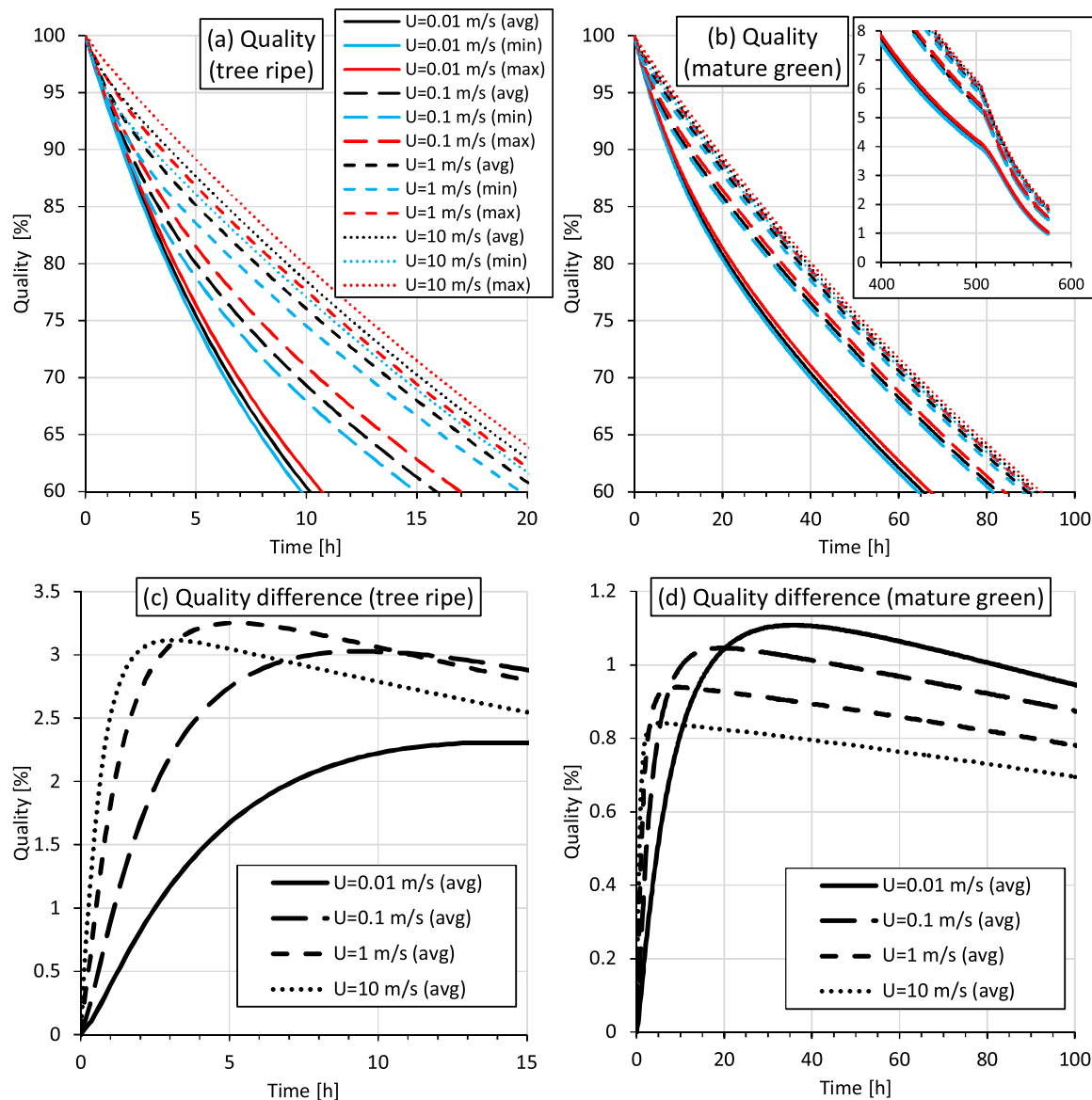


Fig. 8. Overall quality evolution of the fruit pulp (volume-averaged, not including the seed) of tree-ripe (a,c) and mature green (b,d) mangoes as a function of time for different air speeds (avg: average, max: maximal, min: minimal, U: speed), including the difference between minimal and maximal values (c,d). The insert in (b) indicates the period after 21 days of refrigerated transport, when the fruit is brought into unrefrigerated (shelf-life) conditions. The temperatures correspond to those of Fig. 6.

fractional unaccomplished temperature change (Y) was determined:

$$Y = \frac{T_f(t) - T_{ref}}{T_{f,0} - T_{ref}} \quad (9)$$

where subscripts $f,0$ and ref represent the initial temperature of the fruit and the set point temperature in the associated cold chain unit operations, respectively. $T_f(t)$ represents the fruit temperature, which can be, for example, the core temperature at the seed-pulp interface (Fig. 1) or the volume-averaged fruit temperature. From the definition of Y , the seven-eighths cooling/heating time (SECT, $t_{7/8}$) can be determined. The $t_{7/8}$ is the time required to reduce the temperature difference between the initial temperature of the fruit and that of the set point/delivery air by seven-eighths ($Y = 0.125$). The SECT is a useful parameter to characterize the cooling behavior of the fruit in each of the unit operations. The SECT is frequently used in commercial (pre)cooling operations because the fruit temperature at that value is acceptably close to the required storage temperature (Brosnan and Sun, 2001).

2.6. Intercomparison of simulations with cooling experiments on mango fruit

Successful verification of the model was done against empirical correlations for cooling of a sphere (Datta, 2002) (results reported in the Supplementary Material). Also, an intercomparison of the implemented numerical model with cooling experiments on mango fruit in a climatic chamber was also performed. The aim was to experimentally verify the performance of the thermal model of the mango fruit for the accurate prediction of its cooling kinetics. Furthermore, an artificial mango fruit was manufactured, according to the method of (Defraeye et al., 2017) (Fig. 4). This artificial fruit can be considered as the biophysical model counterpart of the digital twin, that is, a biophysical twin of the real mango fruit. Such biophysical twins are specifically developed to enable fruit pulp temperature measurements in a very repeatable way throughout the entire commercial postharvest supply chain. In the present study, cross-validation of the artificial fruit was performed so that it can be applied reliably in commercial chains in the

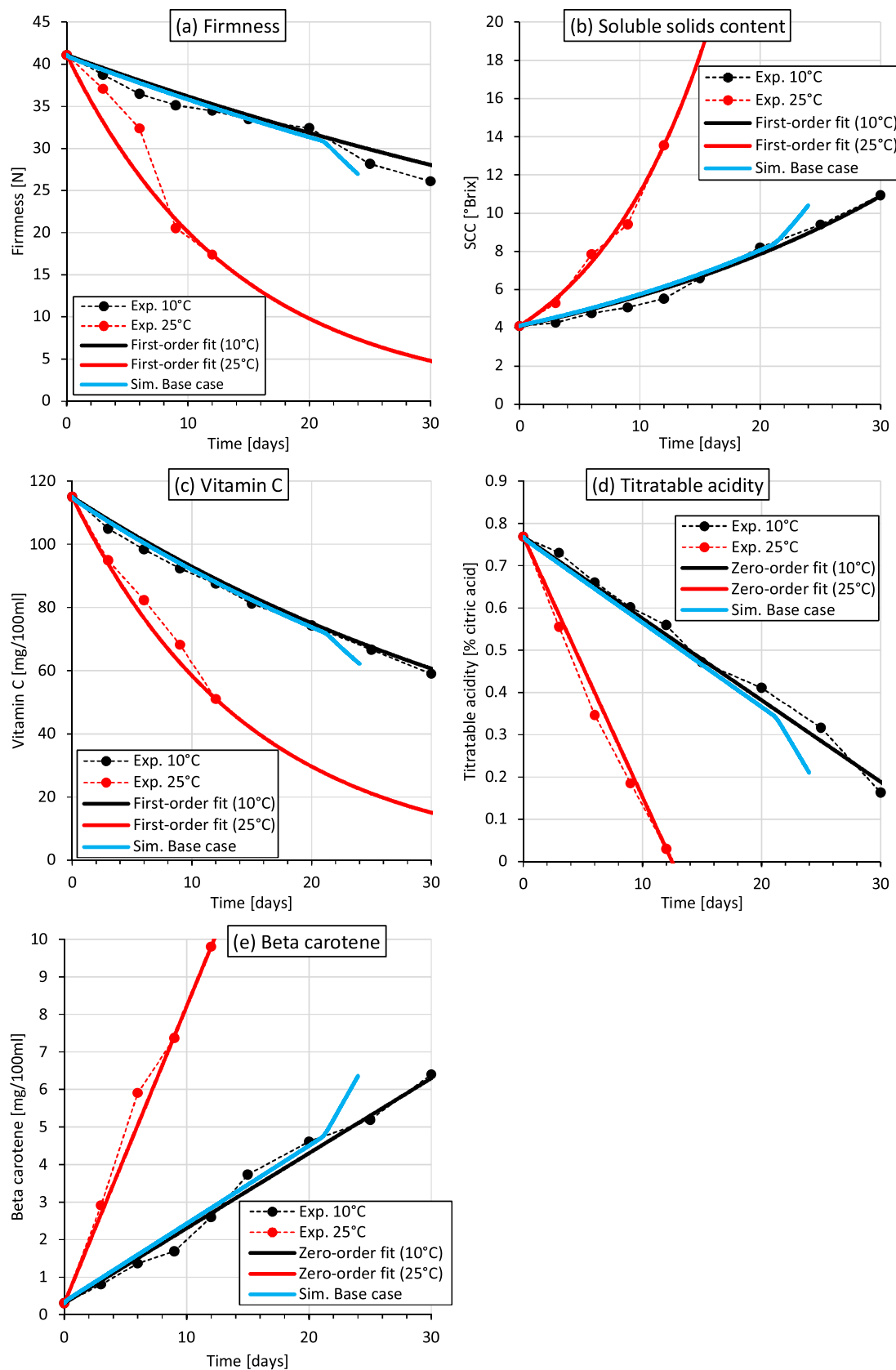


Fig. 9. Fruit quality attributes of the fruit pulp (volume-averaged, not including the seed) for physiologically mature (MG) mangos as a function of time from experiments (Karithi Esther, 2016) (Exp.: experimental), the calibrated kinetic-rate-law model fit which is implemented in the simulations (Section 2.2), and the simulations of the base case (Sim.: simulations).

Table 5

Time constants for the cooling process at different speeds and for fruit quality attributes.

Parameter	Time constant
Cooling	
0.01 m s^{-1}	17.3
0.1 m s^{-1} (base case)	5.1
1 m s^{-1}	1.5
10 m s^{-1}	0.6
Quality	
Storage life – ripe	9.48×10^4
Storage life – mature green	3.79×10^5
Firmness	3.74×10^6
Soluble solids content	-1.80×10^6
Vitamin C	2.72×10^6

future. Climate chamber experiments were conducted with real mango fruit and the biophysical twin, as detailed in the Supplementary Material.

3. Results and discussion

3.1. Intercomparison simulations vs. experiment

In Fig. 5, the core temperature (at the seed-pulp interface, Probe 2 in Fig. 1) over time is shown for the mango fruit, the artificial fruit sensor device and the simulations of the two cooling runs. The data show that the thermal behavior of the artificial fruit sensor device is very similar to the various real mango fruit, as its temperature profile falls well within the data for real fruit. The artificial fruit was thereby successfully engineered to mimic the thermal response of real fruit. A distinct spread within the thermal response of the individual mango fruit can be noticed, indicating the inherent biological variability. The found agreement is similar to the one previously identified when comparing the thermal response of apple fruit with an artificial apple fruit (Defraeye et al., 2017).

The thermal behavior of the digital mango fruit, meaning the computational model, is very similar to its biophysical counterpart, namely the fruit simulator. This finding is somewhat anticipated, as the digital fruit was designed as its real-life equivalent (or vice versa) and so they share a similar thermal response. A good agreement with the real mango fruit is also obtained over the entire cooling period. These

results confirm that the digital mango fruit, given the environmental boundary conditions are known, accurately predicts the conductive heat transfer and convective heat exchange of this complex-shaped composite fruit with the environment. The good agreement between the digital and biophysical models indicates they can be used interchangeably, and both are representative of the thermal response of an average Kent mango fruit.

3.2. Impact of airflow rate

3.2.1. Cooling and heterogeneity

Along with DAT (T_{ref}), the airflow rate is the main driving force for convective heat exchange of the fruit with its environment and thereby will determine fruit quality as well. In Fig. 6, the volume-averaged fruit temperature and the minimal and maximal values are given for airspeeds (U_{ref}) ranging from 0.01 to 10.00 m s^{-1} (Fig. 6a and b), as well as the difference between the minimal and maximal temperatures inside the fruit (Fig. 6c and d). Note that during cooling, the minimal temperature typically corresponds to the fruit surface and the maximal value corresponds to the fruit core (Probe 1 in Fig. 1), which is the last part of the fruit to reach the DAT. The graphs focus on the cooling period and the warming-up, period when the fruit is placed back in ambient conditions, i.e., the shelf life period at the retailer, after being held 21 days in refrigerated storage.

The airspeeds correspond to a Re range ($U_{ref} L_{ref}/\nu_a$) of 68 to 68,000 and Biot numbers ($CHTC_{ref} L_{ref}/\lambda_p$) of 0.3–10.0. These values are based on the length scale L_{ref} (99 mm), U_{ref} , $CHTC_{ref}$ for a sphere, with λ_p denoting the thermal conductivity of the fruit (Table 1). The airflow rate has a large impact on the cooling rate, with SECT equal to 45.8, 11.2, 3.5, and 1.5 h for airflows of 0.01, 0.10, 1.00, and 10.00 m s^{-1} , respectively. For Biot numbers above one, temperature gradients are expected to be present in the fruit during cooling. As such, the conductive heat transport in the fruit also plays a significant role in the cooling kinetics, in addition to the convective heat exchange with the air. Such internal thermal heterogeneity is evident in the data (Figs. 6b and 7) and is higher for high airspeeds, so high Biot numbers. Significant temperature differences within the fruit can be found, which reach even 7 °C for a short time at an airspeed of 10 m s^{-1} .

Note that these temperature heterogeneities within the fruit can become even more pronounced in reality. The reason is the complex turbulent airflow field around the fruit, which results in a variation in convective heat transfer rates (thus CHTCs) over the fruit surface

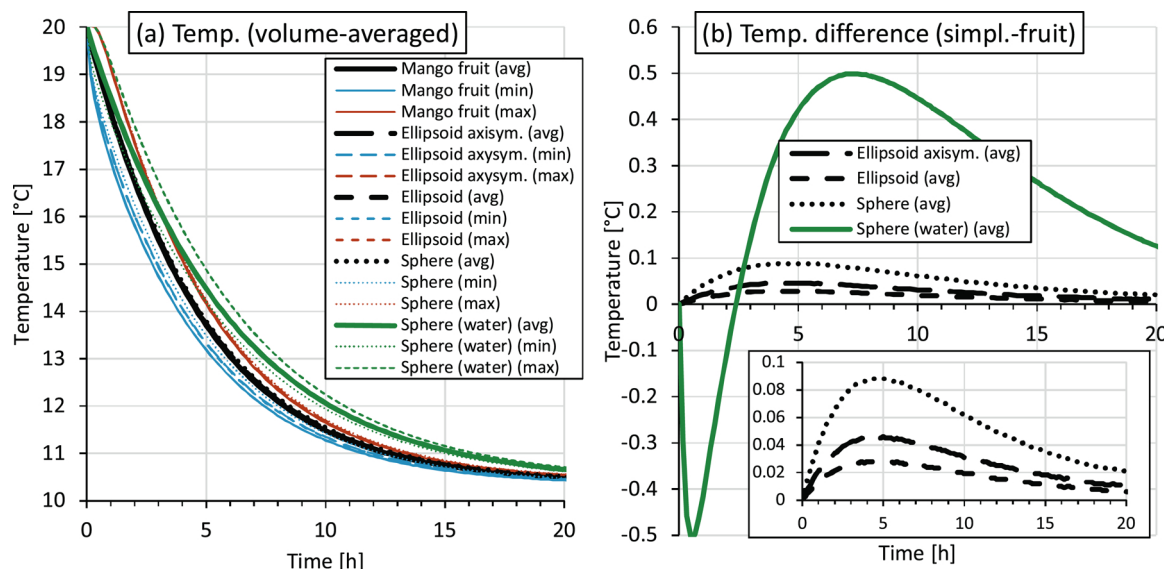


Fig. 10. Volume-averaged fruit temperatures, as well as minimal and maximal values, as a function of time for different geometrical shape simplifications (simpl.-fruit) and for a water-filled sphere. Corresponding differences between minimal and maximal temperatures in the fruit.

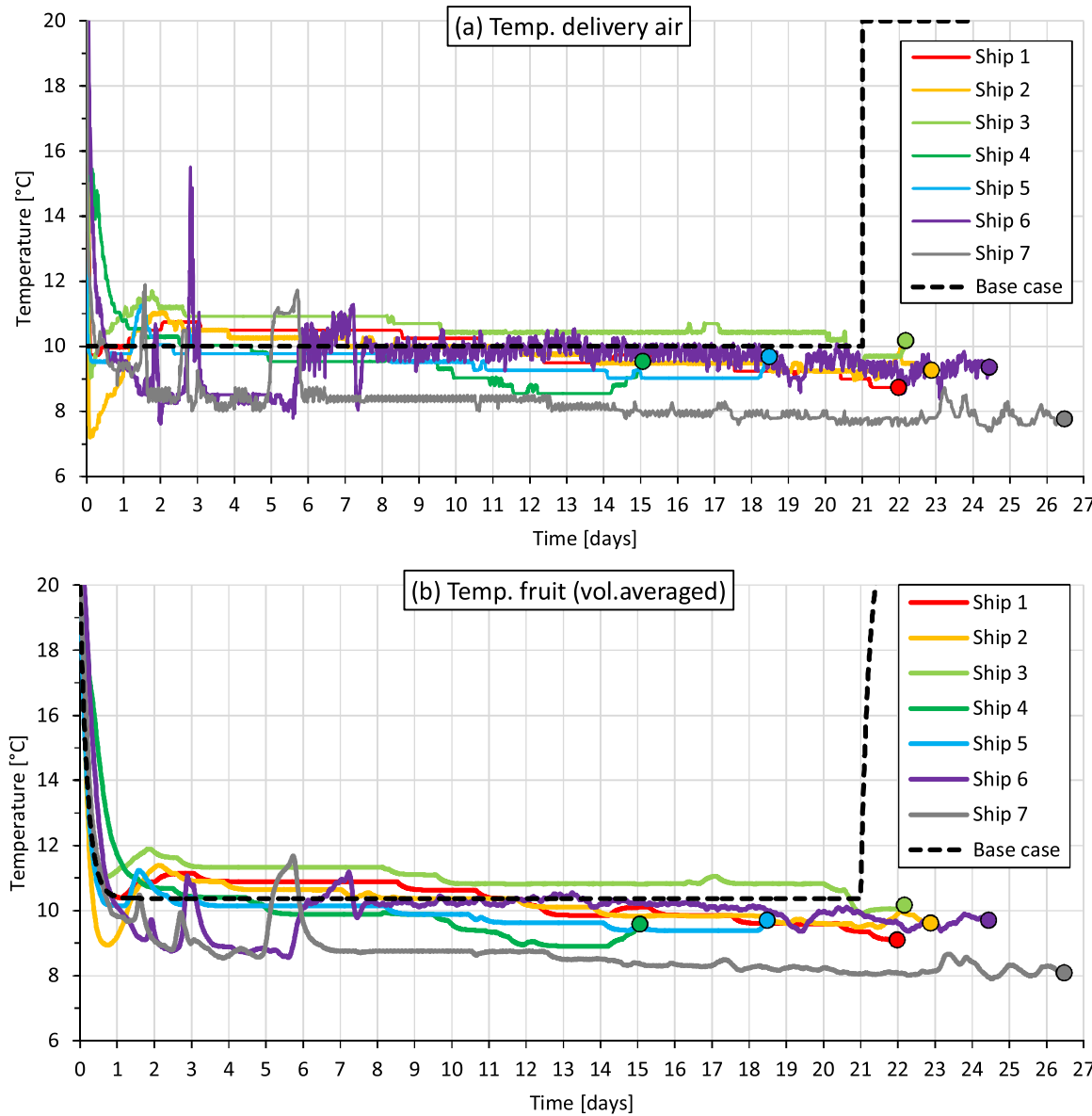


Fig. 11. (a) Air temperature as a function of time, as measured by a sensor in the mango packaging for different maritime shipments, (b) corresponding fruit temperature (volume averaged) calculated by the digital twin. The dots represent the end of each chain.

(windward vs. leeward). In this study, a constant CHTC was assumed over the fruit surface because the airflow was not explicitly solved. A recent study unveiled differences in CHTCs between the trailing and leading edge (Tagliavini et al., 2019). In conclusion, temperature gradients are noticeable (so measurable) in the fruit, especially when cooling at high airspeeds.

3.2.2. Heat of respiration

The impact of the heat of respiration on fruit temperature is apparent from Fig. 6a and b. When the product is completely cooled for transport (after about 30 h for the base case) or heated up again for shelf life conditions, the fruit temperature differs from the DAT due to the heat production from highly respiring fruit. This difference with the DAT is small at high airspeeds, but at low speeds (0.01 m s^{-1}), it increases up to 1.0°C during cooling and to 3.7°C during heating since the produced heat is less easily removed by convection. This difference in final fruit temperatures between cooling and heating emphasizes the temperature dependency of the respiration heat production, wherein fruit produce more heat at a higher temperature. In conclusion, for mango fruit, the heat of respiration will be measurable, especially at

high temperatures, and needs to be included in the modeling. Previous studies on other fruit have mostly neglected the heat of respiration, which is justified for low-respiring fruit (Berry et al., 2016; T. Defraeye et al., 2015a, 2015b, 2015c, 2015d; Wu et al., 2018).

3.2.3. Fruit quality

The temperature history directly affects the evolution of the fruit quality in the cold chain (section 2.2, Eq. (5)). The overall quality evolution of the fruit pulp (not including the seed) of ripe and MG mangos is shown as a function of time in Fig. 8 for different airspeeds (Table 4). Here, the volume-averaged value and the minimal and maximal values are shown. In Fig. 9, the volume-averaged quality attributes of the fruit pulp (not including the seed) are shown in a similar way for physiologically mature (MG) mangos as a function of time, but for a single airspeed since the differences between airspeeds were very small. Only the average values are given because the variation within the fruit was very small and even less than the differences observed in the overall quality (Fig. 8). The experimental data and the model calibration curve at two temperatures are also given for each attribute.

The difference in quality (maximum vs. minimum) between

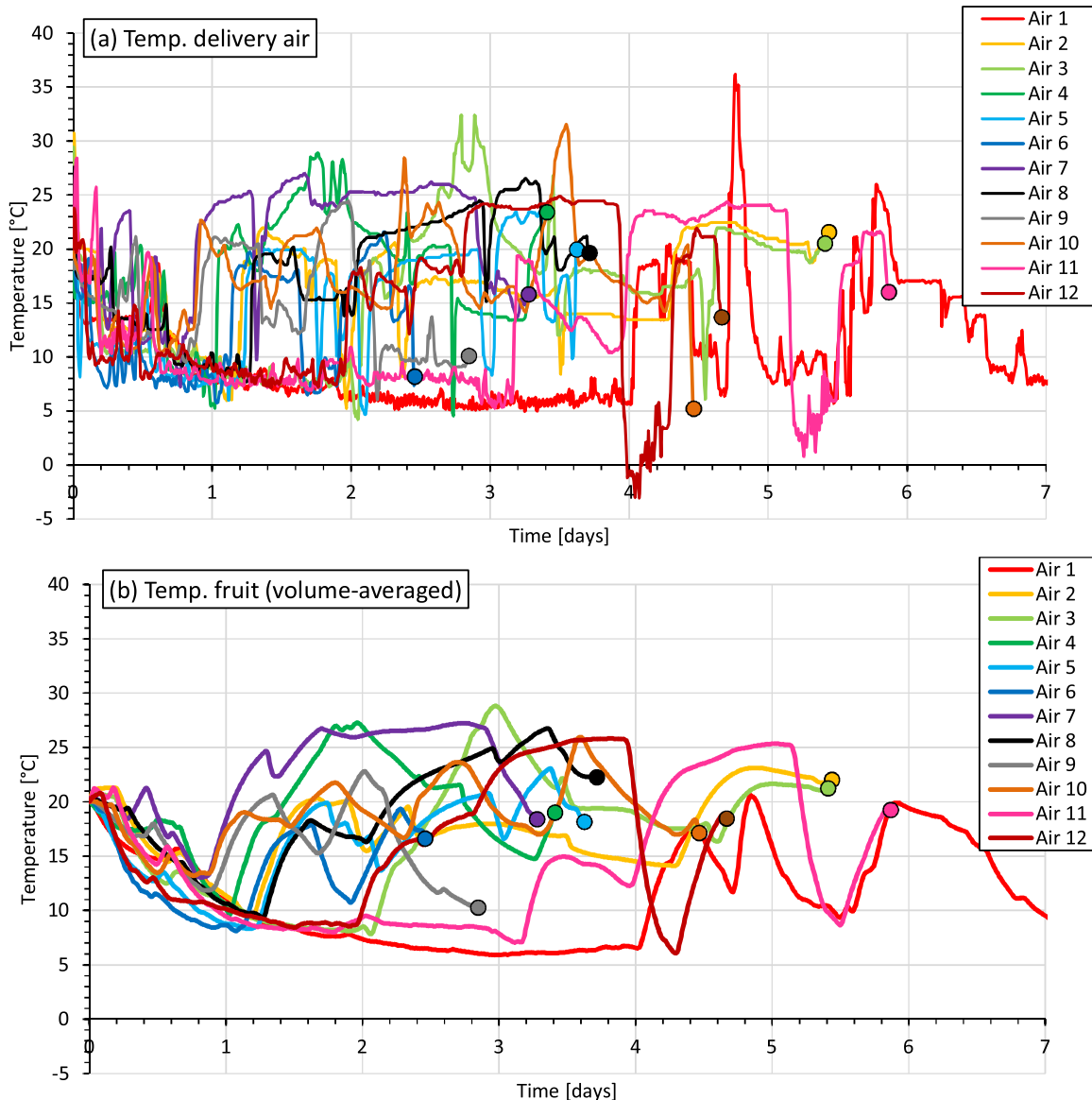


Fig. 12. (a) Air temperature as a function of time, as measured by a sensor in the mango packaging for different airfreight shipments, (b) corresponding fruit temperature (volume averaged) calculated by the digital twin. The dots represent the end of each chain.

different airspeeds is pronounced for ripe mangoes but is much smaller for MG mangos (Fig. 8). The differences inside the fruit only range up to a small percentage for ripe mangos and are quasi-negligible inside MG mangos. For the fruit quality attributes (Fig. 9), a good agreement of the simulations with the experimental data (Karathi Esther, 2016) and the calibrated kinetic rate law model fit (section 2.2) is obtained. Differences are attributed to the cooling process and the heat of respiration. As a result, the fruit does not immediately reach the DAT (10 °C), and also remains at a slightly higher temperature, such that quality decays faster. For the base case, namely physiologically MG mangos, firmness typically drops 10.2 N over the 21 days and an additional 3.9 N during three days at the retailer. The SSC increased by 4.2 and 2.1°Brix, respectively. These fruit quality attributes neither vary noticeably inside a fruit nor with the airspeed (results not shown).

In summary, although the temperature differences between different speeds or within the fruit are quite significant (Figs. 6 and 7), the impact on the resulting fruit quality attributes seems to be much smaller. This phenomenon can be explained by evaluating the time constants of both processes. A time constant for a parameter X is defined, for an exponential function, as:

$$X(t) = X_0 e^{-t/\tau} \quad (10)$$

As the first-order reaction kinetics model proposed above for overall quality, and some individual quality attributes are also described by a similar exponential function (Eq. (7), as $C_i = 0$), the time constant can be derived as $\tau = 1/k_i(T)$, which is calculated from Eq. (8). The temperature-time evolution during cooling can also be described by the following exponential function (Thijs Defraeye et al., 2015a; Thompson, 2008):

$$Y(t) = e^{-Pt} \quad (11)$$

where P is the cooling coefficient. As such, the time constant can be derived as $\tau = 1/P$. A lag-time factor could be included as well, to account for the delay at the start of the cooling process induced by the thermal capacity, but to enable a more straightforward comparison with other time constants, this was not done here. The time constants for the overall quality decay, the different quality attributes (at 15 °C) and for the cooling process (at each speed, based on the volume-averaged fruit temperature, and the temperatures at the start of the cooling process, to have a good fit) are given in Table 5. Note that for quality attributes with zero-order kinetics, no time constant was defined.

The time constants of cooling are much lower—typically more than three orders of magnitude—than those of quality decay, meaning the cooling process is much faster. The time constants for cooling are the largest at low speeds, so these are the closest to those of quality decay. It means that for typical forced convective cooling, the process often happens so fast that differences in cooling rates have a limited impact on quality decay. However, for forced convective cooling in ventilated palletized packaging, high speeds near vent holes, as well as low speeds due to dead zones, can be found. As such, inside a cargo, time constants for cooling can vary significantly in practice, even within a single unit operation.

The riper the fruit, the lower the fruit quality time constant, demonstrating the need to cool ripe fruit faster but also more uniformly. For the quality attributes, all of them are equally susceptible to temperature, having a similar time constant. In summary, it is important to cool at high airflow rates after harvest, especially for riper fruit. However, the quality variations inside the fruit are rather constant and independent of the air-cooling speed.

3.3. Impact of geometrical simplifications

The impact of three simplified geometrical representations of mango fruit (Table 1) on the mango fruit cooling behavior is shown in Fig. 10. Here the volume-averaged fruit temperature (pulp and seed) over time is presented, together with the minimal and maximal values in the fruit, which are representative of the temperature in the fruit core (Probe 1 in Fig. 1) and at the surface (Probe 3 in Fig. 1). All geometrical representations cool very similarly to each other, with differences in SECT of the mango fruit (volume-averaged-temperature-based) below 10 min for the ellipsoid and below 20 min for the sphere. The maximal differences between temperatures were below 0.5 °C. Note that also for higher airflow speeds (10 m s^{-1}), the impact of the shape did not increase significantly (results not reported), with maximal differences between temperatures of the different geometries below 0.6 °C. These differences mainly come from the different shape and distance from the fruit core (or seed), as all have the same volume of the pulp and seed, and so a similar thermal capacity. The reported differences between detailed and simplified geometries are likely to be acceptable for engineering purposes. Simplified shape model representations of mango fruit can, in principle, be used as models for digital and biophysical twins, instead of the full biomimetically-engineered fruit twins (Figs. 1

and 4).

However, the thermal properties of these digital (or artificial fruit) play a critical role. This effect is illustrated by a comparison with the cooling of a water-filled sphere is also made in Fig. 10. Such water-filled spheres have often been used as fruit simulators and, thereby, substitutes for real fruit (De Castro et al., 2005, 2004; Delela et al., 2013). The thermal properties of water, however, do not match those of real fruit (Table 2), as fruit also contains other components, such as carbohydrates and air. From Fig. 10, the water-filled sphere cools much slower than the spherical representation of the mango fruit, with the SECT differing by about 150 min (2.5 h). In conclusion, simplified geometries could be used to simplify the modeling, meshing, and simulation, especially when dealing with large assemblies of fruit. However, it is important that the thermal properties and overall volume are matched for digital and physical twins. In this study, the fruit was evaluated as a single entity. However, when packed in larger bulks, the shape of the fruit will also affect the airflow patterns, thus cooling behavior of the entire shipment (Gruyters et al., 2018). As such, the thermal capacity of the surrounding fruit can induce an additional time lag (Thijs Defraeye et al., 2015a, 2015b, 2015c, 2015d; Wu and Defraeye, 2018).

3.4. Use of digital twin to probe differences between individual supply chains

3.4.1. Maritime vs. Airfreight transport

The idealized cold chain scenarios presented above (e.g., 21 days at a DAT of 10 °C) can be targeted but are never achieved in practice, due to varying DAT and cold chain lengths. Digital twins are used in this section to quantify differences in the thermal history of the fruit pulp and the associated quality attribute evolution throughout multiple cold chains. Two transcontinental pathways are targeted, namely, maritime transport by ship and transport by airfreight. A ship is typically used to transport MG mangos overseas in about three weeks. Air transport is used to export TR mangos in less than one week. The carbon footprint of both pathways can easily differ by a factor of 10 from South America to Europe (Stoessel et al., 2012), with ship transport exhibiting the lowest emissions. The impact of realistic (measured) air temperature profiles on the fruit cooling behavior is shown in Figs. 11 and 12 for multiple maritime and airfreight cold chains. The volume-averaged fruit temperature is also indicated. In Fig. 13, the corresponding

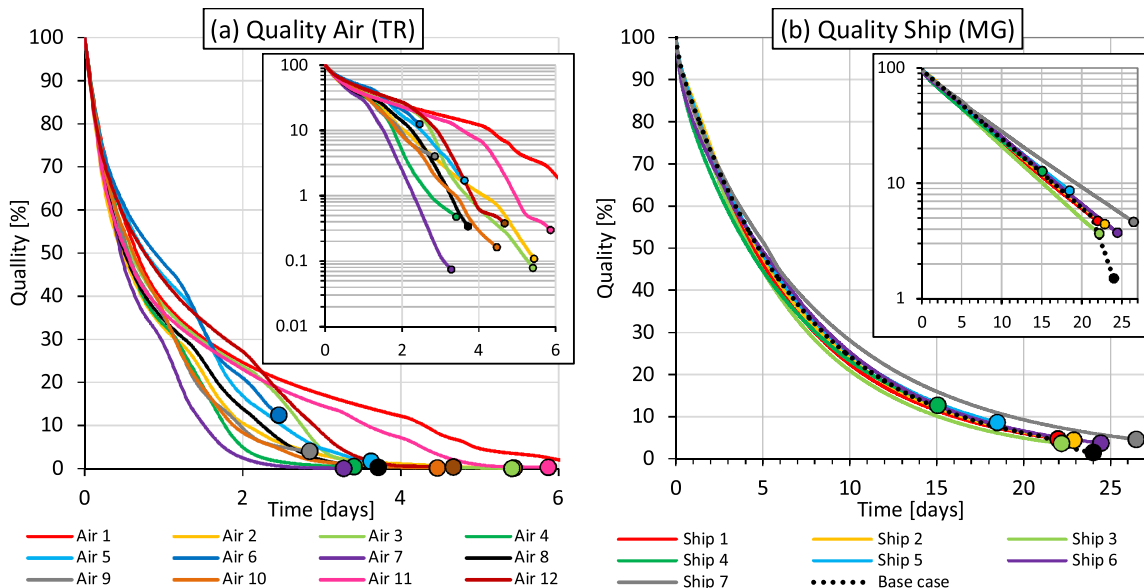


Fig. 13. Quality evolution (calculated from volume-averaged pulp temperature of the digital twin) as a function of time for (a) tree-ripe mangos transported by airfreight, (b) mature green mangos transported by ship. The dots represent the end of each chain.

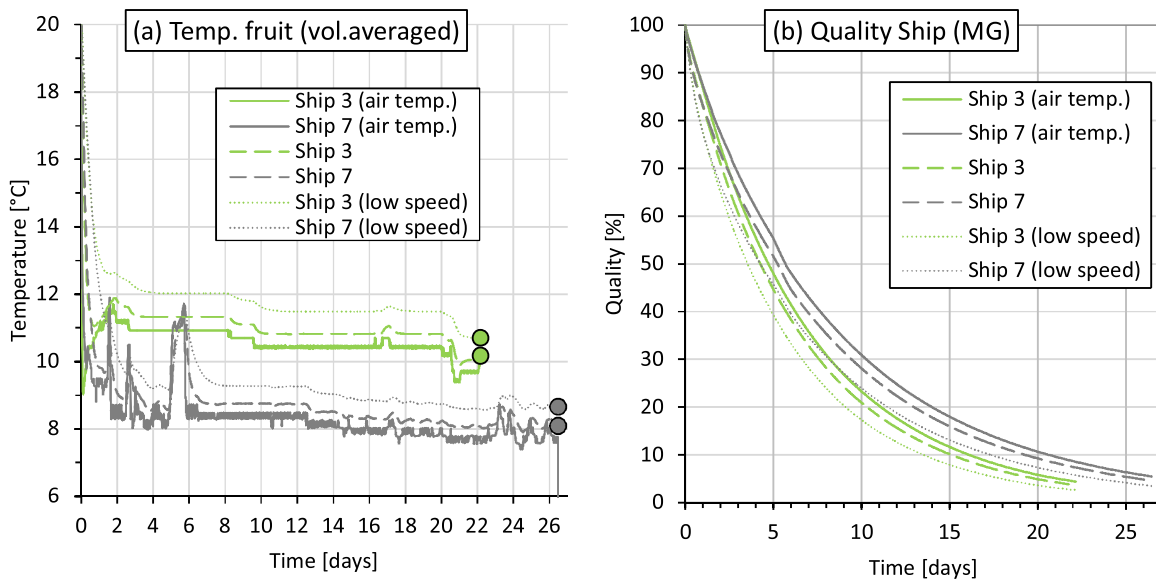


Fig. 14. (a) Fruit temperature (volume averaged) calculated by the digital twin as a function of time for two maritime shipments for two airflow rates, (b) corresponding quality evolution as a function of time for mature-green mangos transported by ship. The quality evolution based on the air temperature is also depicted. The dots represent the end of each chain.

average quality is shown (based on the volume-averaged fruit pulp temperature) for maritime (MG) and airfreight (TR) mangos.

The data show that the air temperature history, as well as the total duration of the trip, vary significantly between different cold chains, especially for airfreight transport. The average temperature between the shipments was 9.6 ± 0.7 °C (standard deviation) for ship transport and 15.6 ± 3.0 °C for air transport. The average duration was 21.6 ± 3.8 days for ship transport and 4.7 ± 2.3 days for air transport. As a result, the fruit temperature also varied considerably between the different shipments. The delay of the fruit's thermal response compared with the air temperature is evident (Figs. 11b and 12b). Due to the thermal inertia of the fruit, peaks in air temperatures are damped out. The variation in temperature history between individual supply chains is also reflected in the resulting fruit quality (Fig. 13).

Note that the threshold value at which the fruit is considered to be fully lost is 1%. Periods with constant temperature, so constant cooling rates, are evident from the logarithmic graphs, as linear regions.

3.4.2. Impact of the speed of the cooling air

The CHTC values used for fruit cooling were estimated based on the assumed airflow rate in the container (Table 4). Refrigerated containers can, however, have different airflow regimes because lower speeds are often used, for example, to save energy. The delay in the thermal response of the fruit to a change in DAT is, nonetheless, closely related to the supplied airflow rate. In Fig. 14, the impact of cooling at lower airflow rates (Table 4) on the volume-averaged fruit temperature and the corresponding average quality is shown for two maritime supply chains of MG mangos. The two airflow rates give a distinct response, which is slower at lower airflow rates. It is important to note that due to the heat of respiration, also in periods of rather constant air temperatures, lower airflow rates lead to higher fruit temperatures. This trend is reflected in a faster quality loss.

3.4.3. Relevance of digital twins for future cold chain optimization

A key question to be answered is what is the added benefit of a digital twin compared with the information that can currently be extracted based on air temperature. One could, for example, easily predict fruit quality evolution based on air temperature alone, using the kinetic rate law models (section 2.2). To explore this aspect, fruit quality predictions based on air temperature—not averaged fruit temperature—have been made. The results are reported in Figs. 14 and 15 for ship and air transport, respectively, together with predictions based on fruit temperature, relying on digital twins.

Marked differences in quality evolution can be found when using air vs. fruit-pulp temperatures. These differences are most pronounced for ripe mangos. In periods of cooling, wherein the air temperature is lower than the fruit temperature, the quality based on air temperature is higher. In periods of warming up of the air, indicated by the arrows for airfreight transport (Fig. 15), the air-temperature-quality predictions catch up with those based on fruit temperatures. The differences not only originate from thermal inertia but are also due to the heat of respiration produced in the fruit, which makes the fruit's temperature slightly higher than the air temperature. Furthermore, the airflow rate has an important impact on fruit quality (Fig. 14), which is not

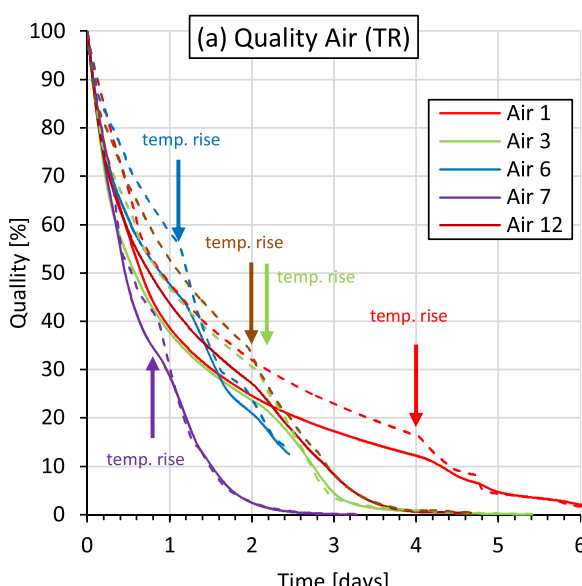


Fig. 15. Quality evolution as a function of time for tree-ripe mangos transported by airfreight for several cold chains, calculated based on the volume-averaged fruit temperature (full line) and on the air temperature (dotted line). Temp. rise indicates that there is a distinct increase or peak in temperature.

apparent if the air temperature is used to quantify the quality evolution.

The identified differences in Figs. 14 and 15 are a very important finding because they indicate the need and potential of digital twins to evaluate product quality and storage life more accurately in fresh produce cold chains. The added accuracy compared with air-temperature-based kinetic rate law modeling is, however, strongly dependent on the species, the fruit's ripeness degree and the airflow rate. In summary, digital twins are especially relevant for perishable species that are stored at low airflow rates (e.g., in container or storage room). The particular advantages of the physics-based digital twin are that temperature and quality attribute data are available at the high spatial and temporal resolution, local peaks in temperatures are captured, which could be important for chilling injury, for example, and the contribution of respiratory heat due to the metabolism is quantified accurately.

4. Conclusions and outlook

Digital fruit twins were used to quantify the thermal history and associated biochemical quality evolution throughout transcontinental supply chains. These twins were coupled with the real-world environmental conditions, via offline-measured air temperature data. The digital twin was successfully validated against real mango fruit and a biophysical fruit twin, namely, a fruit simulator sensor device. Our main findings are the following:

- Based on measured environmental conditions, digital twins identified the impact of unique cold chain length and delivery air temperature history for different transport pathways (maritime vs. air-freight). Digital twins helped to record and understand the differences in thermal history of individual shipments.
- Digital twins are particularly instrumental for supply chains of very perishable species (e.g., ripe mangoes, berries) that are stored at low airflow rates (e.g., in container or storage room).
- Significant differences in temperatures and temperature gradients were found at different airspeeds. The impact of airspeed on the resulting fruit quality attributes was much smaller, due to the differences in time scales between cooling and quality decay.
- More simplified shape-model representations of mango fruit can be used for digital and biophysical twins, but it is imperative that the thermal properties and overall volume are matched.
- For mango fruit, the heat of respiration was noticeable, especially at high temperatures, so this heat production term needs to be included in the digital twin as well.

This twin enables us to predict where the quality loss of complex-shaped fruit with internal features (e.g. seed), occurs for every individual cold chain, even with strongly varying environmental conditions. In that way, digital twins can help to improve refrigeration processes and logistics to reduce food losses, thereby making the refrigerated food supply chain greener. The digital twin model will be enhanced in the future to include moisture loss via the fruit skin due to evaporation. In addition to the increased decay due to elevated temperatures, low-temperature damage, such as chilling injury, should also be included. In the future, the digital twin should also run in real-time, driven by real-time-measured temperature data.

Author contributions

T.D. conceptualized the study, wrote the project proposals to secure funding and did project administration; A.B. also contributed to writing the project proposal 26032.1 PFLS-LS; T.D. developed the methodology, with key input from G.T. for the simulations and fruit quality evolution and S.S. for the environmental measurements and quality assessment; W.W., K.P., P.V., and M.A.K. fabricated the artificial fruit simulator and performed the corresponding experiments; T.D.

performed data collection, analysis, interpretation and visualization of the simulation results; T.D. performed supervision of W.W., G.T., and K.P.; P.V. performed supervision of M.A.K.; T.D. wrote the original draft; the other authors critically reviewed and edited the manuscript.

Acknowledgements

We acknowledge the support of the Swiss National Science Foundation SNSF (project 200021_169372) and of the Commission for Technology and Innovation (CTI, Switzerland, projects 18155.2 PFLS-LS, 26032.1 PFLS-LS).

Appendix A. Supplementary data

Supplementary material related to this article can be found, in the online version, at doi:<https://doi.org/10.1016/j.resconrec.2019.06.002>.

References

- Ambaw, A., Verboven, P., Defraeye, T., Tijskens, E., Schenk, A., Opara, U.L., Nicolai, B.M., 2013. Porous medium modeling and parameter sensitivity analysis of 1-MCP distribution in boxes with apple fruit. *J. Food Eng.* 119. <https://doi.org/10.1016/j.jfoodeng.2013.05.007>.
- ASHRAE, 2010. ASHRAE Handbook - Refrigeration: Systems and Applications (SI Edition). Atlanta.
- Baldwin, E.A., Burns, J.K., Kazakas, W., Brecht, J.K., Hagenmaier, R.D., Bender, R.J., Pesis, E., 1999. Effect of two edible coatings with different permeability characteristics on mango (*Mangifera indica* L.) ripening during storage. *Postharvest Biol. Technol.* 17, 215–226. [https://doi.org/10.1016/S0925-5214\(99\)00053-8](https://doi.org/10.1016/S0925-5214(99)00053-8).
- Berry, T.M., Defraeye, T., Nicolai, B.M., Opara, U.L., 2016. Multiparameter analysis of cooling efficiency of ventilated fruit cartons using CFD: impact of vent hole design and internal packaging. *Food Bioprocess Technol.* 9. <https://doi.org/10.1007/s11947-016-1733-y>.
- Bon, J., Váquiro, H., Benedito, J., Telis-Romero, J., 2010. Thermophysical properties of mango pulp (*Mangifera indica* L. cv. Tommy Atkins). *J. Food Eng.* 97, 563–568. <https://doi.org/10.1016/j.jfoodeng.2009.12.001>.
- Brecht, J.K., Chau, K.V., Fonseca, S.C., Oliveira, F.A.R., Silva, F.M., Nunes, M.C.N., Bender, R.J., 2003a. Maintaining optimal atmosphere conditions for fruits and vegetables throughout the postharvest handling chain. *Postharvest Biol. Technol.* 27, 87–101. [https://doi.org/10.1016/S0925-5214\(02\)00185-0](https://doi.org/10.1016/S0925-5214(02)00185-0).
- Brecht, J.K., Chau, K.V., Fonseca, S.C., Oliveira, F.A.R., Silva, F.M., Nunes, M.C.N., Bender, R.J., 2003b. Maintaining optimal atmosphere conditions for fruits and vegetables throughout the postharvest handling chain. *Postharvest Biol. Technol.* 27, 87–101. [https://doi.org/10.1016/S0925-5214\(02\)00185-0](https://doi.org/10.1016/S0925-5214(02)00185-0).
- Brosnan, T., Sun, D.W., 2001. Precooling techniques and applications for horticultural products - a review. *Int. J. Refrig.* 24, 154–170.
- Cantre, D., Herremans, E., Verboven, P., Ampofo-Asiamah, J., Hertog, M.L.A.T.M., Nicolai, B.M., 2017. Tissue breakdown of mango (*Mangifera indica* L. Cv. Carabao) due to chilling injury. *Postharvest Biol. Technol.* 125, 99–111. <https://doi.org/10.1016/j.postharvbio.2016.11.009>.
- Casado, C., Marugán, J., Timmers, R., Muñoz, M., Grieken, R., Van, 2017. Comprehensive multiphysics modeling of photocatalytic processes by computational fluid dynamics based on intrinsic kinetic parameters determined in a differential photoreactor. *Chem. Eng. J.* 310, 368–380. <https://doi.org/10.1016/j.cej.2016.07.081>.
- Clary, B.L., 1960. Convective Heat Transfer Coefficients From Ellipsoidal Models and Irregular Shapes to Air. PhD thesis. University of Georgia.
- Copelli, S., Barozzi, M., Petrucci, N., Casson, V., Tecnologia, A., Vico, V.G.B., 2019. Modeling and process optimization of a full-scale emulsion polymerization reactor. *Chem. Eng. J.* 358, 1410–1420. <https://doi.org/10.1016/j.cej.2018.10.055>.
- Datta, A.K., 2002. Biological and Bioenvironmental Heat and Mass Transfer, 1st ed. New York. <https://doi.org/10.1201/9780203910184>.
- De Castro, L.R., Vigneault, C., Cortez, L.A.B., 2004. Container opening design for horticultural produce cooling efficiency. *Food, Agric. Environ.* 2, 135–140.
- De Castro, L.R., Vigneault, C., Cortez, L.A.B., 2005. Effect of container openings and airflow rate on energy required for forced-air cooling of horticultural produce. *Can. Biosyst. Eng.* 47, 1–9.
- De Mello Vasconcelos, O.C., Duarte, D., de CastroSilva, J., Mesa, N.F.O., Teruel Mederos, J.B., de Freitas, S.T., 2019. Modeling 'Tommy Atkins' mango cooling time based on fruit physicochemical quality. *Sci. Hortic. (Amsterdam)* 244, 413–420. <https://doi.org/10.1016/j.scientia.2018.09.068>.
- Dea, S., Brecht, J.K., Nunes, M.C.N., Baldwin, E.A., 2010. Occurrence of chilling injury in fresh-cut "Kent" mangoes. *Postharvest Biol. Technol.* 57, 61–71. <https://doi.org/10.1016/j.postharvbio.2010.02.005>.
- Defraeye, Thijss, Cronjé, P., Berry, T., Opara, U.L., East, A., Hertog, M., Verboven, P., Nicolai, B., 2015a. Towards integrated performance evaluation of future packaging for fresh produce in the cold chain. *Trends Food Sci. Technol.* 44, 201–225. <https://doi.org/10.1016/j.tifs.2015.04.008>.
- Defraeye, T., Cronjé, P., Verboven, P., Opara, U.L., Nicolai, B., 2015d. Exploring ambient loading of citrus fruit into reefer containers for cooling during marine transport using

- computational fluid dynamics. *Postharvest Biol. Technol.* 108, 91–101. <https://doi.org/10.1016/j.postharvbio.2015.06.004>.
- Defraeye, Thijs, Cronjé, P., Verboven, P., Opara, U.L.U.L., Nicolai, B., 2015b. Exploring ambient loading of citrus fruit into reefer containers for cooling during marine transport using computational fluid dynamics. *Postharvest Biol. Technol.* 108, 91–101. <https://doi.org/10.1016/j.postharvbio.2015.06.004>.
- Defraeye, T., Verboven, P., Nicolai, B., 2013. CFD modelling of flow and scalar exchange of spherical food products: turbulence and boundary-layer modelling. *J. Food Eng.* 114. <https://doi.org/10.1016/j.jfoodeng.2012.09.003>.
- Defraeye, Thijs, Verboven, P., Opara, U.L.U.L., Nicolai, B., Cronjé, P., 2015c. Feasibility of ambient loading of citrus fruit into refrigerated containers for cooling during marine transport. *Biosyst. Eng.* 134, 20–30. <https://doi.org/10.1016/j.biosystemseng.2015.03.012>.
- Defraeye, T., Wu, W., Prawiranto, K., Fortunato, G., Kemp, S., Hartmann, S., Cronje, P., Verboven, P., Nicolai, B., 2017. Artificial fruit for monitoring the thermal history of horticultural produce in the cold chain. *J. Food Eng.* 215, 51–60. <https://doi.org/10.1016/j.jfoodeng.2017.07.012>.
- Dehghannya, J., Ngadi, M., Vigneault, C., 2010. Mathematical modeling procedures for airflow, heat and mass transfer during forced convection cooling of produce: a review. *Food Eng. Rev.* 2, 227–243. <https://doi.org/10.1007/s12393-010-9027-z>.
- Delele, M.A., Ngcobo, M.E.K., Getahun, S.T., Chen, L., Mellmann, J., Opara, U.L., 2013. Studying airflow and heat transfer characteristics of a horticultural produce packaging system using a 3-D CFD model. Part I: model development and validation. *Postharvest Biol. Technol.* 86, 536–545. <https://doi.org/10.1016/j.postharvbio.2013.08.014>.
- Emongor, V.E., 2015. The effects of temperature on storage life of mango (*Mangifera indica* L.). *Am. J. Exp. Agric.* 5, 252–261. <https://doi.org/10.9734/AJEA/2015/12174>.
- FAO, 2018. Statistics Division of the Food and Agriculture Organization of the United Nations. [WWW Document]. URL <http://www.fao.org/faostat/en/> (accessed 7.26.18). FAOSTAT.
- Gartner, 2019a. 5 Trends Emerge in the Gartner Hype Cycle for Emerging Technologies. pp. 2018. [WWW Document]. URL <https://www.gartner.com/smarterwithgartner/5-trends-emerge-in-gartner-hype-cycle-for-emerging-technologies-2018/> (Accessed 1.29.19).
- Gartner, 2019b. Prepare for the Impact of Digital Twins [WWW Document]. URL <https://www.gartner.com/smarterwithgartner/prepare-for-the-impact-of-digital-twins/> (Accessed 1.29.19).
- Gill, P.P.S., Jawandha, S.K., Kaur, N., Singh, N., 2017. Physico-chemical changes during progressive ripening of mango (*Mangifera indica* L.) cv. Dashehari under different temperature regimes. *J. Food Sci. Technol.* 54, 1964–1970. <https://doi.org/10.1007/s13197-017-2632-6>.
- Gruyters, W., Verboven, P., Diels, E., Rogge, S., Smeets, B., Ramon, H., Defraeye, T., Nicolai, B., 2018. Modelling cooling of packaged fruit using 3D shape models. *Food Bioprocess Technol.* 11, 2008–2020. <https://doi.org/10.1007/s11947-018-2163-9>.
- Gustavsson, J., Cederberg, C., Sonesson, U., van Otterdijk, R., Meybeck, A., 2011. Global Food Losses and Food Waste: Extend, Causes and Prevention. Rome, Italy.
- Gwanpua, S.G., Verboven, P., Leducq, D., Brown, T., Verlinden, B.E., Bekele, E., Aregawi, W., Evans, J., Foster, A., Duret, S., Hoang, H.M., Van Der Sluis, S., Wissink, E., Hendriksen, L.J.A.M., Taoukis, P., Gogou, E., Stahl, V., El Jabri, M., Le Page, J.F., Claussen, I., Indergaard, E., Nicolai, B.M., Alvarez, G., Geeraerd, A.H., 2015. The FRISBEE tool, a software for optimising the trade-off between food quality, energy use, and global warming impact of cold chains. *J. Food Eng.* 148, 2–12. <https://doi.org/10.1016/j.jfoodeng.2014.06.021>.
- Kader, A., 1997. Mango - Recommendations for Maintaining Postharvest Quality. [WWW Document]. UC Davis Commodity fact sheets. URL http://postharvest.ucdavis.edu/Commodity_Resources/Fact_Sheets/Datastores/Fruit_English/?uid=37&ds=798 (Accessed 6.27.18).
- Karithi Esther, M., 2016. Evaluation of the efficacy of Coolbot™ cold storage technology to preserve quality and extend shelf life of mango fruits. University of Nairobi.
- Marcelo, D., Orbegoso, E.M., Olivares, J., Olivares, R.L.M., 2018. Numerical Characterization of the Thermal-fluid Behavior of a Typical “mangoes-crate” System Working in a Hot-water Treatment Scenario. *Dyna* 7.
- Mendoza Orbegoso, E.M., Villar-Yacila, P., Marcelo, D., Oquelis, J., 2017. Improvements in thermal performance of mango hot-water treatment equipments: data analysis, mathematical modelling and numerical-computational simulation. *J. Sustain. Dev. Energy, Water Environ. Syst.* 5, 219–239. <https://doi.org/10.13044/j.sdwes.d5>.
- 0145.
- Mohammed, M., Brecht, J.K., 2002. Reduction of chilling injury in “Tommy Atkins” mangoes during ripening. *Sci. Hortic. (Amsterdam)*. 95, 297–308. [https://doi.org/10.1016/S0304-4238\(02\)00041-9](https://doi.org/10.1016/S0304-4238(02)00041-9).
- Nakamura, N., Rao, D.V.S., Shiina, T., Nawa, Y., 2004. Respiration properties of tree-ripe mango under CA condition. *Jpn. Agric. Res. Q. Jarq* 38, 221–226.
- National Mango Board, 2010. National Mango Board Sustainability Assessment. 2010. . Ngamchachit, P., Barrett, D.M., Mitcham, E.J., 2014. Effects of 1-Methylcyclopropane and hot water quarantine treatment on quality of “Keitt” mangoes. *J. Food Sci.* 79, 505–509. <https://doi.org/10.1111/1750-3841.12380>.
- Nordio, M., Rizzi, F., Manzolini, G., Mulder, M., Raymakers, L., 2019. Experimental and modelling study of an electrochemical hydrogen compressor. *Chem. Eng. J.* 369, 432–442. <https://doi.org/10.1016/j.cej.2019.03.106>.
- Norton, T., Tiwari, B., Sun, D.W., 2013. Computational fluid dynamics in the design and analysis of thermal processes: a review of recent advances. *Crit. Rev. Food Sci. Nutr.* 53, 251–275. <https://doi.org/10.1080/10408398.2010.518256>.
- Nunes, M.C.N., Emond, J.P., Brecht, J.K., Dea, S., Proulx, E., 2007. Quality curves for mango fruit (cv. Tommy Atkins and Palmer) stored at chilling and nonchilling temperatures. *J. Food Qual.* 30, 104–120.
- Pesis, E., Aharoni, D., Aharon, Z., Ben-Arie, R., Aharoni, N., Fuchs, Y., 2000. Modified atmosphere and modified humidity packaging alleviates chilling injury symptoms in mango fruit. *Postharvest Biol. Technol.* 19, 93–101. [https://doi.org/10.1016/S0925-5214\(00\)00080-6](https://doi.org/10.1016/S0925-5214(00)00080-6).
- Radu, A.I., Bergwerff, L., Loosdrecht, M.C.M., Van Picioreanu, C., 2014. A two-dimensional mechanistic model for scaling in spiral wound membrane systems. *Chem. Eng. J.* 241, 77–91. <https://doi.org/10.1016/j.cej.2013.12.021>.
- Rao, D.V.S., Shivashankara, K.S., 2014. Individual shrink wrapping extends the storage life and maintains the antioxidants of mango (cv. ‘Alphonso’ and ‘Bangana palli’) stored at 8 °C. *J. Food Sci. Technol.* 52, 4351–4359. <https://doi.org/10.1007/s13197-014-1468-6>.
- Robertson, G.L., 2016. Food Packaging: Principles and Practice, third edition, third. ed. Taylor & Francis Group LLC, Boca-Raton. <https://doi.org/10.1177/0340035206070163>.
- Sitaraman, H., Kuhn, E.M., Nag, A., Sprague, M.A., Tucker, M.P., Stickel, J.J., 2015. Multiphysics modeling and simulation of high-solids dilute-acid pretreatment of corn stover in a steam-explosion reactor. *Chem. Eng. J.* 268, 47–59. <https://doi.org/10.1016/j.cej.2015.01.020>.
- Sivakumar, D., Van Deventer, F., Terry, L.A., Polenta, G.A., Korsten, L., 2012. Combination of 1-methylcyclopropane treatment and controlled atmosphere storage retains overall fruit quality and bioactive compounds in mango. *J. Sci. Food Agric.* 92, 821–830. <https://doi.org/10.1002/jsfa.4653>.
- Slaughter, D.C., 2009. Methods for Management of Ripening in Mango: a Review of Literature.
- Stoessel, F., Jurasko, R., Pfister, S., Hellweg, S., 2012. Life cycle inventory and carbon and water footprint of fruits and vegetables: Application to a Swiss retailer. *Environ. Sci. Technol.* 46, 3253–3262. <https://doi.org/10.1021/es2030577>.
- Tagliavini, G., Defraeye, T., Carmeliet, J., 2019. Multiphysics modeling of convective cooling of non-spherical fruit to unveil quality evolution throughout the cold chain. Submitted.
- Thompson, 2008. Commercial Cooling of Fruits, Vegetables and Flowers. University of California, University of California, California.
- Thompson, J.F., 2004. Pre-cooling and storage facilities. In: USDA (Ed.), USDA Agriculture Handbook Number 66: The Commercial Storage of Fruits, Vegetables, and Florist and Nursery Stocks. USDA, pp. 1–10.
- Van Boekel, M.A.J.S., 2008. Kinetic modeling of food quality: a critical review. *Compr. Rev. Food Sci. Food Saf.* 7, 144–158. <https://doi.org/10.1111/j.1541-4337.2007.00036.x>.
- Whitaker, S., 1972. Forced convection heat transfer correlations for flow in pipes, past flat plates, single cylinders, single spheres, and for flow in packed beds and tube bundles. *AIChE J.* 18, 361–371.
- Wu, W., Cronjé, P., Nicolai, B., Verboven, P., Linus Opara, U., Defraeye, T., 2018. Virtual cold chain method to model the postharvest temperature history and quality evolution of fresh fruit – A case study for citrus fruit packed in a single carton. *Comput. Electron. Agric.* 144, 199–208. <https://doi.org/10.1016/j.compag.2017.11.034>.
- Wu, W., Defraeye, T., 2018. Identifying heterogeneities in cooling and quality evolution for a pallet of packed fresh fruit by using virtual cold chains. *Appl. Therm. Eng.* 133, 407–417. <https://doi.org/10.1016/j.applthermaleng.2017.11.049>.